

Esterification of ethanol and lactic acid with WO_3 on montmorillonite catalysts for
ethyl lactate production



A Thesis Submitted in Partial Fulfillment of the Requirements
for the Degree of Master of Engineering in Chemical Engineering

Department of Chemical Engineering

FACULTY OF ENGINEERING

Chulalongkorn University

Academic Year 2020

Copyright of Chulalongkorn University

เอสเทอร์ฟิเคชันของเอทานอลและกรดแลคติกด้วยตัวเร่งปฏิกิริยาทั้งสแตนออกไซด์บนมอนต์มอริลโล
ไนต์เพื่อผลิตเอทิลแลคเตท



วิทยานิพนธ์นี้เป็นส่วนหนึ่งของการศึกษาตามหลักสูตรปริญญาวิศวกรรมศาสตรมหาบัณฑิต
สาขาวิชาวิศวกรรมเคมี ภาควิชาวิศวกรรมเคมี
คณะวิศวกรรมศาสตร์ จุฬาลงกรณ์มหาวิทยาลัย
ปีการศึกษา 2563
ลิขสิทธิ์ของจุฬาลงกรณ์มหาวิทยาลัย

Thesis Title Esterification of ethanol and lactic acid with WO₃ on
montmorillonite catalysts for ethyl lactate production
By Miss Suthicha Mukjinda
Field of Study Chemical Engineering
Thesis Advisor Professor BUNJERD JONGSOMJIT, Ph.D.

Accepted by the FACULTY OF ENGINEERING, Chulalongkorn University in
Partial Fulfillment of the Requirement for the Master of Engineering

..... Dean of the FACULTY OF
ENGINEERING
(Professor SUPOT TEACHAVORASINSKUN, Ph.D.)

THESIS COMMITTEE

..... Chairman
(Associate Professor SORADA KANOKPANONT, Ph.D.)

..... Thesis Advisor
(Professor BUNJERD JONGSOMJIT, Ph.D.)

..... Examiner
(CHUTIMON SATIRAPIPATHKUL, Ph.D.)

..... External Examiner
(Assistant Professor Sasiradee Jantasee, Ph.D.)

สุทธิชา มุขจินดา : เอสเทอร์ิฟิเคชันของเอทานอลและกรดแลคติกด้วยตัวเร่งปฏิกิริยา
 ทั้งสแตนออกไซด์บนมอนต์มอริลโลไนต์เพื่อผลิตเอทิลแลคเตท . (Esterification of
 ethanol and lactic acid with WO_3 on montmorillonite catalysts for ethyl
 lactate production) อ.ที่ปรึกษาหลัก : ศ. ดร.บรรเจิด จงสมจิตร

งานวิจัยนี้มีวัตถุประสงค์เพื่อศึกษาคุณลักษณะ ประสิทธิภาพและเสถียรภาพของตัวเร่งปฏิกิริยา
 ทั้งสแตนออกไซด์ 13.5 เปอร์เซ็นต์ โดยน้ำหนักบนมอนต์มอริลโลไนต์ (W/MMT) ที่อุณหภูมิการสังเคราะห์ตัวเร่ง
 ปฏิกิริยาที่แตกต่างกัน 3 ค่า คือ 375 (W/MMT375), 475 (W/MMT475) และ 575 (W/MMT575) องศา
 เซลเซียส ถูกทดสอบเร่งปฏิกิริยาเอสเทอร์ิฟิเคชันของเอทานอลและกรดแลคติกที่อุณหภูมิ 80 องศา
 เซลเซียส จากการศึกษาคุณลักษณะพบว่าตัวเร่งปฏิกิริยา W/MMT475 มีค่าความเป็นกรดสูงสุด รองมาคือ
 W/MMT375 และ W/MMT575 ตามลำดับ อย่างไรก็ตามพบว่าค่าพื้นที่ผิวของตัวเร่งปฏิกิริยา W/MMT375 มีค่า
 สูงที่สุด รองมาคือ W/MMT475 และ W/MMT575 ตามลำดับ และเมื่อนำตัวเร่งปฏิกิริยาทั้งหมดไปศึกษาด้าน
 ประสิทธิภาพต่อความว่องไวกับปฏิกิริยาเอสเทอร์ิฟิเคชันของเอทานอลและกรดแลคติกพบว่า ตัวเร่งปฏิกิริยา
 W/MMT375 ให้ค่าผลผลิตของเอทิลแลคเตทสูงที่สุดอยู่ที่ 43.2 เปอร์เซ็นต์โดยน้ำหนัก จากนั้นได้ทำการปรับปรุง
 ตัวเร่งปฏิกิริยาให้มีประสิทธิภาพมากขึ้นโดยการสังเคราะห์ตัวเร่งปฏิกิริยา W/MMT375 และใส่ตัวส่งเสริมที่
 ต่างกัน 2 ตัว ได้แก่ เซอร์โคเนียม (W-Zr/MMT375) และ แพลทินัม (W-Pt/MMT375) เพื่อศึกษา
 คุณลักษณะและประสิทธิภาพของตัวเร่งปฏิกิริยา พบว่า W-Pt/MMT375 มีค่าความเป็นกรดและค่าพื้นที่ผิวของ
 ตัวเร่งปฏิกิริยาสูงที่สุด และเมื่อนำตัวเร่งปฏิกิริยาทั้งหมดไปทดสอบประสิทธิภาพต่อความว่องไวกับปฏิกิริยาเอ
 สเทอร์ิฟิเคชันของเอทานอลและกรดแลคติกพบว่า W-Pt/MMT375 ให้ค่าผลผลิตของเอทิลแลคเตทสูงที่สุดอยู่ที่
 48 เปอร์เซ็นต์โดยน้ำหนัก และสุดท้ายได้ทำการศึกษาความเสถียรภาพของตัวเร่งปฏิกิริยา W/MMT375 และ W-
 Pt/MMT375 ด้วยปฏิกิริยาเอสเทอร์ิฟิเคชันของเอทานอลและกรดแลคติกจำนวน 3 รอบ พบว่า ค่าผลผลิตของ
 เอทิลแลคเตทมีการลดลงตามจำนวนรอบที่ทำปฏิกิริยาเพิ่มขึ้น จากการศึกษาคุณลักษณะของตัวเร่งปฏิกิริยา
 W/MMT375 และ W-Pt/MMT375 หลังจากทำปฏิกิริยาแต่ละรอบพบว่าโครงสร้างภายนอกของตัวเร่งปฏิกิริยา
 ไม่ได้รับผลกระทบจากการทดสอบปฏิกิริยา แต่การลดลงของค่าผลผลิตของเอทิลแลคเตทมีผลมาจากค่าปริมาตร
 ความเป็นกรดชนิดสูงสุดลดลงอย่างมีนัยสำคัญ

สาขาวิชา วิศวกรรมเคมี
 ปีการศึกษา 2563

ลายมือชื่อนิสิต
 ลายมือชื่อ อ.ที่ปรึกษาหลัก

6270296321 : MAJOR CHEMICAL ENGINEERING

KEYWORD: ESTERIFICATION, ETHYL LACTATE, MONTMORILLONITE, TUNGSTEN OXIDE,
PROMOTER

Suthicha Mukjinda : Esterification of ethanol and lactic acid with WO_3 on montmorillonite catalysts for ethyl lactate production. Advisor: Prof. BUNJERD JONGSOMJIT, Ph.D.

This research aims to study the characteristics, catalytic properties and stability of tungsten oxide (13.5 wt%) supported on montmorillonite (W/MMT) catalysts prepared by using three different calcination temperatures including 375 (W/MMT375), 475 (W/MMT475) and 575 (W/MMT 575) °C. All catalysts were examined in esterification of ethanol and lactic acid at 80 °C. Characterization studies showed that the W/MMT475 catalyst exhibited the highest acidity, followed by W/MMT375 and W/MMT575, respectively. However, from the surface area result, W/MMT375 exhibited the highest surface area, followed by W/MMT475 and W/MMT575, respectively. When all catalysts were tested in esterification of ethanol and lactic acid, it revealed that the W/MMT375 catalyst was found to have the highest yield of ethyl lactate around 43.2 %. Then, the suitable catalyst (W/MMT375) was further improved by adding two different promoters such as zirconium (W-Zr/MMT375) and platinum (W-Pt/MMT375). Based on NH_3 temperature-programmed desorption, it indicated that the W-Pt/MMT375 catalyst had the highest acidity. When two catalysts were tested in esterification of ethanol and lactic acid, the result showed that the W-Pt/MMT 375 catalyst exhibited higher yield of ethyl lactate (ca.48 %) than W-Zr/MMT 375. Finally, the catalytic stability of the catalysts including W/MMT 375 and W-Pt/MMT 375 was performed around 3 cycles in esterification of ethanol and lactic acid. It was found that the yield of ethyl lactate for each reuse was decreased. The characteristics of the spent W/MMT 375 and W-Pt/MMT 375 catalysts after each cycle up on the catalyst external structure, which is perhaps related to textural properties of catalyst did not affect by the reaction test within 3 cycles of reuse. However, the decrease of moderate to strong acid site related with the catalytic activity was significant.

Field of Study: Chemical Engineering

Student's Signature

Academic Year: 2020

Advisor's Signature

ACKNOWLEDGEMENTS

I would like to gratefully my sincere thanks to my advisor Prof. Bunjerd Jongsomjit, Ph.D. to give advice, suggestion, guidance and supported during experimentation and discussion to accomplish my thesis. I am most grateful for his teaching and advice. This thesis cannot be achieved without my advisor.

In addition, I will also be grateful to thesis committees is Asst. Prof. Sorada Kanokpanont, Ph.D. as a chairman, Chutimon Satirapipathkul, Ph.D. as an examiner and Asst. Prof. Sasiradee Jantasee, Ph.D. as an external examiner for a good suggestion to improve thesis research.

I would like to thank members and scientists in Center of Excellence on Catalysis and Catalytic Reaction Engineering laboratory, Chulalongkorn University and Cat-react industrial project for the financial support of this project.

Finally, I would like to gratefully acknowledge my parents, who always pay attention, continuous support, and encouragement for everyday since I studied in master's degree. I also thank to friend and senior for carefulness, continued support, kind suggestion and useful help.



จุฬาลงกรณ์มหาวิทยาลัย
CHULALONGKORN UNIVERSITY

Suthicha Mukjinda

TABLE OF CONTENTS

	Page
.....	iii
ABSTRACT (THAI).....	iii
.....	iv
ABSTRACT (ENGLISH).....	iv
ACKNOWLEDGEMENTS.....	v
TABLE OF CONTENTS.....	vi
LIST OF TABLES.....	x
LIST OF FIGURES.....	xii
CHAPTER 1.....	1
INTRODUCTION.....	1
1.1 Introduction.....	1
1.2 Objective.....	2
1.3 Research scopes.....	2
1.4 Research methodology.....	4
1.5 Research plan.....	7
CHAPTER 2.....	8
THEORY AND LITERATURE REVIEWS.....	8
2.1 Ethyl lactate.....	8
2.2 Lactic acid.....	9
2.3 Esterification of ethyl lactate.....	10
2.4 Amberlyst-15.....	12

2.5 Montmorillonite clay (MMT catalyst).....	13
2.6 Ammonium metatungstate (AMT)	13
2.7 Tungsten trioxide.....	14
2.8 Promoter	15
2.8.1 Zirconium (IV) oxynitrate hydrate.....	16
2.8.2 Platinum (II) acetylacetonate	16
2.9 Literature reviews.....	17
CHAPTER 3.....	21
EXPERIMENTAL	21
3.1 Materials.....	21
3.2 Catalyst preparation	22
3.3 Catalyst characterization.....	22
3.3.1 Powder X-ray diffraction (XRD).....	22
3.3.2 Fourier-transform infrared spectroscopy (FTIR)	22
3.3.3 N ₂ physisorption (BET).....	23
3.3.4 Scanning electron microscope (SEM) and energy dispersive X-ray spectroscopy (EDX)	23
3.3.5 Temperature-programmed desorption of ammonia (NH ₃ -TPD).....	23
3.3.6 X-ray photoelectron spectroscopy (XPS).....	23
3.3.7 X-ray fluorescence (XRF)	24
3.4 Catalytic activities and stabilities	24
3.4.1 Calibration of reactants, products.....	24
3.4.2 Esterification reaction of ethanol with lactic acid.....	24
3.4.3 Analysis and calculation.....	26

CHAPTER 4.....	27
RESULT AND DISCUSSION.....	27
4.1 The optimal calcination temperature selection.....	27
4.1.1 Catalyst characterization.....	27
4.1.1.1 X-ray Powder Diffraction (XRD).....	27
4.1.1.2 Fourier-transform infrared spectroscopy (FTIR).....	28
4.1.1.3 N ₂ physisorption (BET).....	30
4.1.1.4 Scanning electron microscope (SEM) and Energy dispersive X-ray spectroscopy (EDX).....	34
4.1.1.5 Temperature-programmed desorption of ammonia (NH ₃ -TPD).....	35
4.1.1.6 X-ray photoelectron spectroscopy (XPS).....	36
4.1.1.7 X-ray fluorescence (XRF).....	38
4.1.2 Catalytic activities.....	38
4.1.3 Summary.....	39
4.2 The suitable promoter selection.....	40
4.2.1 Catalyst characterization.....	40
4.2.1.1 X-ray Powder Diffraction (XRD).....	40
4.2.1.2 Fourier-transform infrared spectroscopy (FTIR).....	41
4.2.1.3 N ₂ physisorption (BET).....	42
4.2.1.4 Scanning electron microscope (SEM) and Energy dispersive X-ray spectroscopy (EDX).....	45
4.2.1.5 Temperature-programmed desorption of ammonia (NH ₃ -TPD).....	46
4.2.1.6 X-ray photoelectron spectroscopy (XPS).....	46
4.2.2 Catalytic activities.....	48

4.2.3 Summary.....	49
4.3 The study of stability of catalysts.....	50
4.3.1 Catalytic stability.....	50
4.3.2 Catalyst characterizations	52
4.3.2.1 Scanning electron microscope (SEM)	52
4.3.2.2 Temperature-programmed desorption of ammonia (NH ₃ -TPD).....	53
4.3.3 Summary.....	54
CHAPTER 5.....	55
CONCLUSION AND RECOMMENDATION	55
5.1 Conclusions	55
5.2 Recommendations	56
REFERENCES	57
APPENDIX A.....	64
APPENDIX B	65
APPENDIX C	68
APPENDIX D.....	69
VITA.....	70

LIST OF TABLES

	Page
Table 1 Properties of ethyl lactate.....	9
Table 2 Properties of lactic acid.....	10
Table 3 Properties of Amberlyst-15	12
Table 4 Properties of ammonium metatungstate.....	14
Table 5 Properties of tungsten trioxide.....	15
Table 6 Properties of Zirconium (IV) oxynitrate hydrate	16
Table 7 Properties of Platinum (II) acetylacetonate	16
Table 8 The chemicals used in the catalyst preparation	21
Table 9 The chemicals used in the calibration of reactants and product	24
Table 10 The operating condition of gas chromatography (GC).....	25
Table 11 FTIR assignments according to wavenumber (cm^{-1}) of MMT and W/MMT catalysts.....	29
Table 12 Properties of MMT and W/MMT catalysts.....	30
Table 13 Elemental distribution of montmorillonite clays (MMT 375, MMT 475 and MMT 575) and W/MMT catalysts obtained by EDX.....	35
Table 14 The amount of acidity of tungsten supported on montmorillonite clays (W/MMT 375, W/MMT 475 and W/MMT 575) by NH_3 -TPD compared with Amberlyst-15	36
Table 15 XPS signals distribution of montmorillonite clays all temperature (MMT 375, MMT 475 and MMT 575) and tungsten supported on montmorillonite clays all temperature (W/MMT 375, W/MMT 475 and W/MMT 575)	37

Table 16 Surface compositions of montmorillonite clays all temperature (MMT 375, MMT 475 and MMT 575) and tungsten supported on montmorillonite clays all temperature (W/MMT 375, W/MMT 475 and W/MMT 575) by XPS	37
Table 17 XRF analysis result of W/MMT catalysts.....	38
Table 18 FTIR assignments of W/MMT 375, W-Zr/MMT 375 and W-Pt/MMT 375.....	42
Table 19 Properties of W-Zr/MMT 375 and W-Pt/MMT 375 catalysts compared with W/MMT 375 catalyst	43
Table 20 Element distribution of W-Zr/MMT 375 and W-Pt/MMT 375 catalysts.....	46
Table 21 The amount of acidity of W-Zr/MMT 375 and W-Pt/MMT catalysts by NH ₃ -TPD	46
Table 22 XPS signals distribution of W-Zr/MMT 375.....	47
Table 23 XPS signals distribution of W-Pt/MMT 375.....	47
Table 24 Surface composition of W-Zr/MMT 375	47
Table 25 Surface composition of W-Pt/MMT 375	48
Table 26 The amount of acidity of all catalysts for 3 cycles of reuse as W-Zr/MMT 375 and W-Pt/MMT catalysts obtained by NH ₃ -TPD	54

LIST OF FIGURES

	Page
Figure 1 Chemical formula of ethyl lactate [10].....	8
Figure 2 Structures of lactic acid [10].....	10
Figure 3 Chemical formula of substance in system a) Lactic acid (L_1), b) Lactic acid oligomers (L_{n+1}), c) Ethyl lactate (EL_1), d) Ethyl lactate oligomers (EL_{n+1}) [3, 10].....	11
Figure 4 Structures of Amberlyst-15 [14].....	12
Figure 5 The structure of montmorillonite clay (A) Side view and (B) Top view of MMT [16].....	13
Figure 6 Flow chart of esterification reaction of ethanol with lactic acid.....	25
Figure 7 X-ray powder diffraction patterns of various MMT and W/MMT catalysts calcined at different temperatures.....	28
Figure 8 FTIR spectra of MMT and W/MMT catalysts.....	29
Figure 9 N_2 adsorption-desorption isotherm of MMT 375	31
Figure 10 N_2 adsorption-desorption isotherm of MMT 475	31
Figure 11 N_2 adsorption-desorption isotherm of MMT 575	32
Figure 12 N_2 adsorption-desorption isotherm of W/MMT 375	32
Figure 13 N_2 adsorption-desorption isotherm of W/MMT 475	33
Figure 14 N_2 adsorption-desorption isotherm of W/MMT 575	33
Figure 15 The morphologies of montmorillonite clays all temperature (MMT 375, MMT 475 and MMT 575) and tungsten supported on montmorillonite clays all temperature (W/MMT 375, W/MMT 475 and W/MMT 575) measured by SEM at mag. X2,000	34
Figure 16 comparison of ethyl lactate conversion between Amberlyst-15 with W/MMT catalysts calcined at different temperatures (375, 475 and 575 °C)	39

Figure 17 XRD patterns of the W-Zr/MMT 375 and W-Pt/MMT 375 catalysts	41
Figure 18 FTIR spectra of W/MMT 375, W-Zr/MMT 375 and W-Pt/MMT 375 catalysts	42
Figure 19 N ₂ adsorption-desorption isotherm of W-Zr/MMT 375.....	44
Figure 20 N ₂ adsorption-desorption isotherm of W-Pt/MMT 375.....	44
Figure 21 The morphologies of various promoter Zr and Pt for synthesized catalyst tungsten supported on montmorillonite (W-Zr/MMT, W-Pt/MMT) calcined at temperature 375 °C measured by SEM at mag. X6,000 (top and bottom left) and at mag. X2,000 (top and bottom right).....	45
Figure 22 The comparison of yield of ethyl lactate between Amberlyst-15 with W/MMT 375, W-Zr/MMT 375 and W-Pt/MMT 375.....	49
Figure 23 The comparison of yield of ethyl lactate between Amberlyst-15 with W/MMT 375 and W-Pt/MMT 375 from the fresh, 1 st reuse, 2 nd reuse and 3 rd reuse catalyst in esterification.....	51
Figure 24 The comparison of an efficiency of catalyst reusability in ethyl lactate production between Amberlyst-15 with W/MMT 375 and W-Pt/MMT 375 from the fresh, 1 st reuse, 2 nd reuse and 3 rd reuse in esterification.....	51
Figure 25 The morphologies of all catalysts after tested in the reaction around 3 cycles measured by SEM at mag. X100 (For both of Amberlyst-15 ^a and Amberlyst-15 ^b) and at mag. X2,000	53

CHAPTER 1

INTRODUCTION

1.1 Introduction

At present, Ethanol product from biomass is material generally used as feedstocks in Thailand, which is sugarcane, molasses (by-product from cane sugar processing), and cassava roots by fermentation process. Fermentation is the most common method for producing fuel ethanol [1]. And most of the ethanol in the country is converted and mixed with fuel oil for gasohol use in vehicles including fuel types such as E10, E20 and E85. Currently, the demand of ethanol as energy and substance use in various industries is highly increasing. However, in the near future the increase in ethanol production will exceed in the demand, which leads to the decline in ethanol prices. Therefore, it is interesting to convert ethanol into higher value chemicals. Thus, converting ethanol into a higher value product can significantly help moderate this problem [2].

Ethyl lactate is interesting because it is an important organic ester that is efficient and environmental friendly, non-volatile biodegradable, non-carcinogenic and non-ozone depleting also it found that has been applied to many industries such as food, additive, fragrance flavoring chemicals and solvents. Ethyl lactate is a product from esterification reaction of ethanol with lactic acid using homogenous catalyst such as sulfuric acid (H_2SO_4) for this reaction. Furthermore, popular commercial heterogeneous catalyst such as Amberlyst-15, which is the mostly used catalyst in this process due to its high selectivity for esterification reaction. However, it still has high price and also reusability problem for this catalyst (low efficiency of regenerate). Therefore, it is tended to synthesize the other catalysts to replace Amberlyst-15 for lower price and better reusability (high efficiency of regenerate) [3]. It is known that montmorillonite clay is one of the most interesting acid catalysts because it has moderate surface area and high acidity [4]. Moreover, the montmorillonite clay can be found in nature especially in the northern part of Thailand (it was found around 2 million tons base on 2020 year), thus it is low price and also environmentally friendly catalyst.

Accordingly, this research targets to investigate the montmorillonite clay as catalyst for mesopore catalyst agent. On the other hand, the catalyst is still needed to improve for better acidity for the esterification in order to have higher catalytic activity, which is favored for this reaction. Mostly, the catalyst is loaded with metal oxide to improve catalytic properties of acidity such as tungsten trioxide (WO_3), zirconium dioxide (ZrO_2), and titanium dioxide (TiO_2) [5, 6]. Furthermore, it is ravishing to deposit the metal promoter onto catalyst to increase catalytic activity in order to have higher acidity of catalyst, which is essential for esterification reaction [7].

In present study, the effects of tungsten loading over montmorillonite catalyst were investigated. In addition, different calcination temperatures for prepared catalysts and choose the best temperature for loading metal promoters improvement were also investigated in order to evaluate the catalytic activity and perhaps textural and chemical changes in the final catalyst. The catalysts were characterized using various characterization techniques. After selecting the optimal calcination temperature, the catalyst was loaded with different promoters such as Zr and Pt. Then, selection of the best promoter loaded on catalyst was studied in esterification of ethanol with lactic acid in a batch reactor at $80\text{ }^\circ\text{C}$, pressure 1 atm, the molar ratio of reactants (ethanol/lactic acid at 3:1) and reaction time for 4 h. Finally, comparative deactivation test of catalyst with and without promoter was also investigated for stability test and reusable of catalysts.

1.2 Objective

To investigate the effect of calcination temperature for synthesis of tungsten (VI) oxide loading on montmorillonite clay catalysts and metal promoters to compare the catalytic activity (yield of ethyl lactate) in esterification of ethanol with lactic acid to ethyl lactate.

1.3 Research scopes

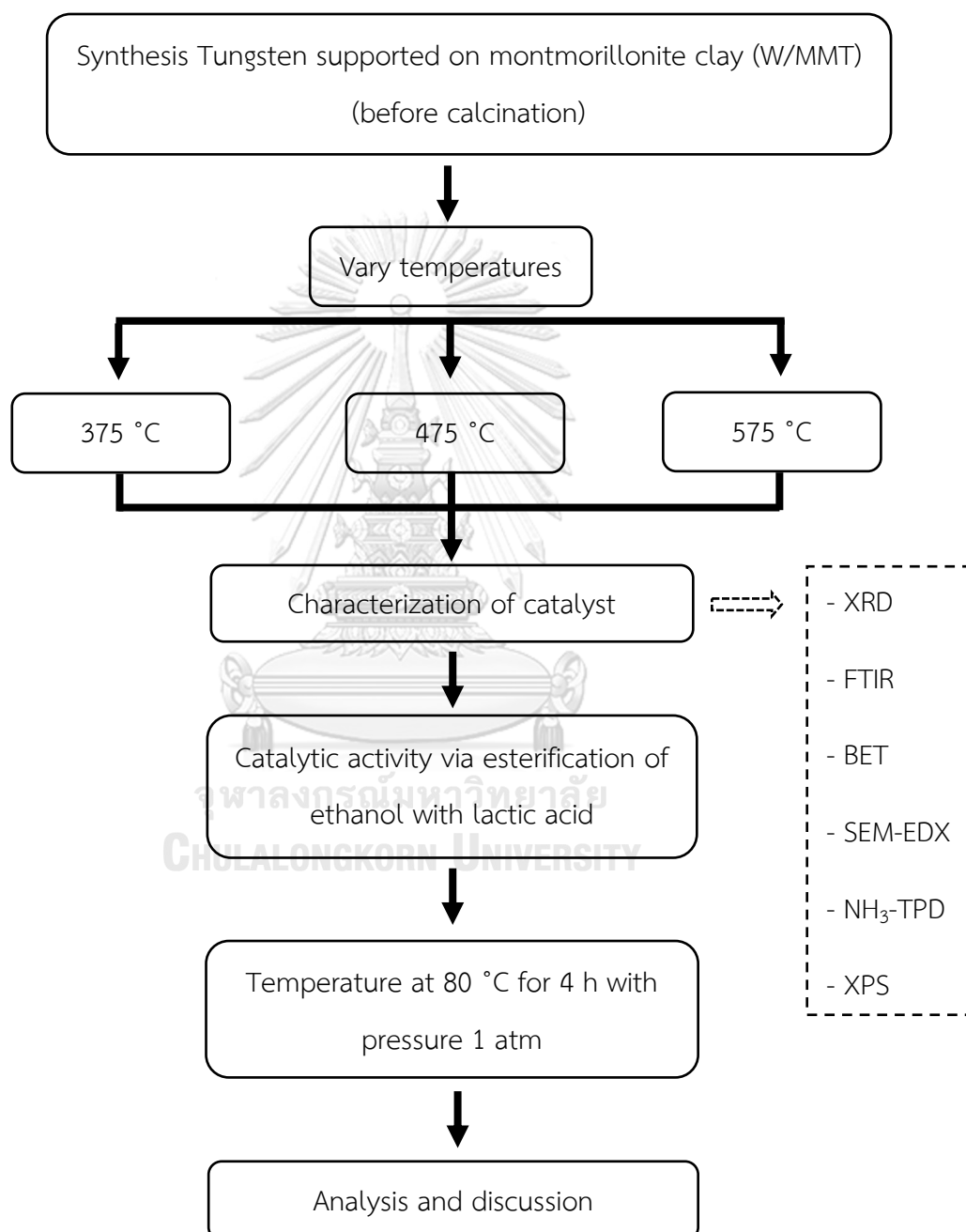
1. Preparation of tungsten (VI) oxide loading on montmorillonite clay catalyst (W/MMT) by incipient wetness impregnation method.

2. Characterization of W/MMT catalyst with powder X-ray diffraction (XRD), N₂ physisorption (BET), Fourier-transform infrared spectroscopy (FTIR), temperature-programmed desorption of ammonia (NH₃-TPD), scanning electron microscope (SEM) and energy dispersive X-ray spectroscopy (EDX), X-ray photoelectron spectroscopy (XPS) and X-ray fluorescence (XRF).
3. To examine of the catalytic activity of synthesis catalyst (W/MMT) and compare with commercial catalyst as Amberlyst-15 in esterification of ethanol with lactic acid at 80°C under pressure 1 atm, molar ratio of reactants (ethanol/lactic acid at 3:1) for 4 h with stirring speed of 700 rpm.
4. To investigate the effect of calcination temperature at 375, 475 and 575°C for synthesis of W/MMT catalyst and compare the catalytic activity in esterification of ethanol with lactic acid at 80°C under pressure 1 atm, the molar ratio of reactants (ethanol/lactic acid at 3:1) for 4 h with stirring speed of 700 rpm.
5. Choose the best calcination temperature for improvement catalyst via loading metal promoters between Zr and Pt and also compare of catalytic activity in esterification of ethanol with lactic acid at 80°C under pressure 1 atm, molar ratio of reactants (ethanol/lactic acid at 3:1) for 4 h with speed 700 rpm.
6. To study deactivation of catalyst between catalyst without promoter and catalyst with the best promoter via stability test.

1.4 Research methodology

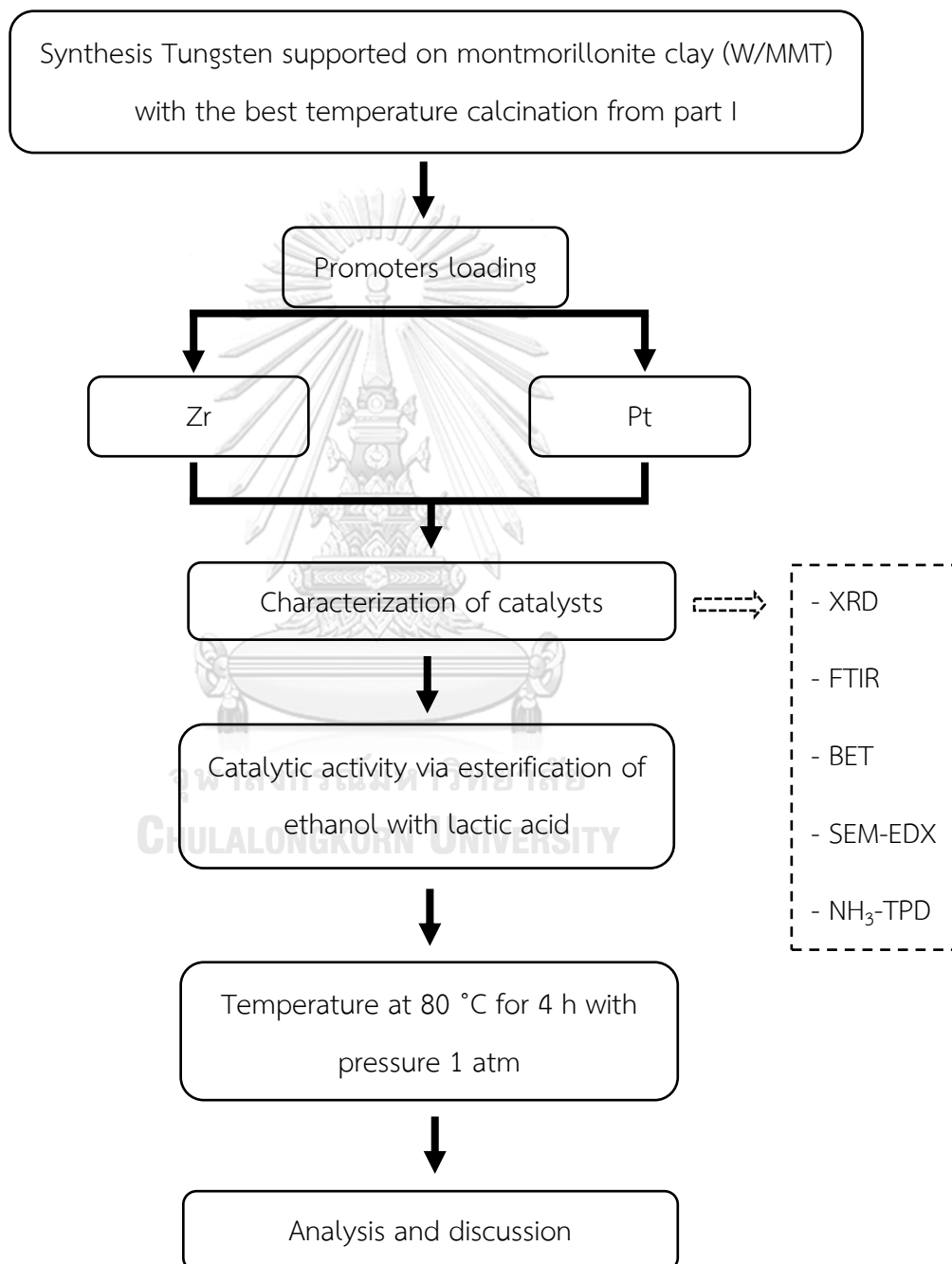
Part I: The optimal calcination temperature selection

Synthesis of tungsten supported on montmorillonite clay and vary calcination temperatures. In addition, catalytic activity is also performed with esterification.



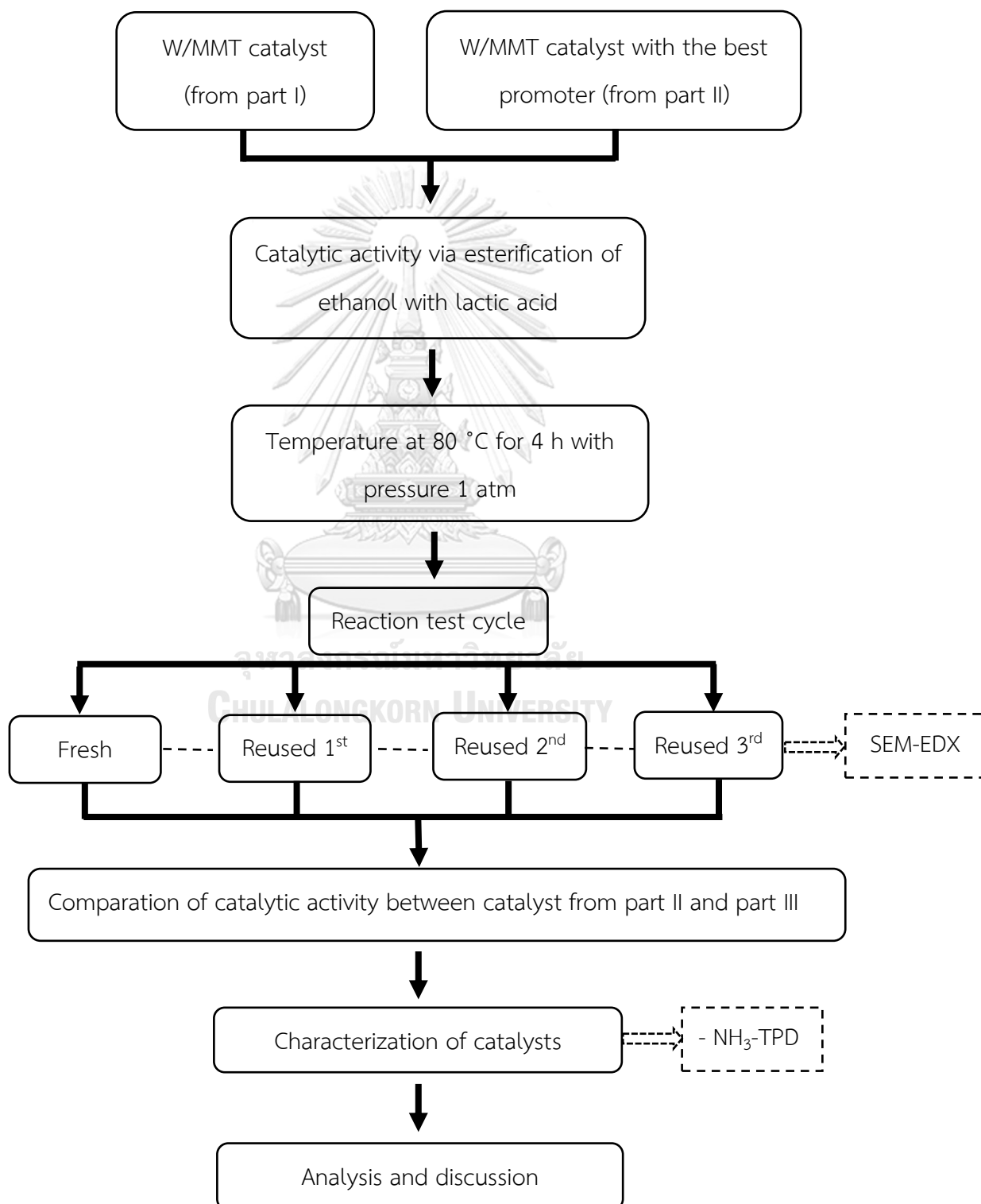
Part II: The suitable promoter selection

Synthesis of tungsten supported on montmorillonite clay with the best calcination temperature and vary the metal promoters. In addition, catalytic activity is also performed with esterification.



Part III: The study of stability of catalysts

Synthesis of tungsten supported on montmorillonite clay with the best calcination temperature compared with the best calcination temperature and promoter. In addition, catalytic activity is also performed with esterification.



1.5 Research plan

Activity	2020							2021					
	6	7	8	9	10	11	12	1	2	3	4	5	6
1. Literature reviews													
2. Synthesis of Tungsten supported on montmorillonite clay													
3. Testing catalytic activity of catalyst via esterification by ethanol with lactic acid													
4. Testing different temperature calcination for preparation of catalyst													
5. Characterization of catalysts from item 4													
6. Testing catalytic activity and stability of catalyst, which gives the highest lactic acid conversion via esterification													
7. Testing different promoter loading on catalyst from item 4													
8. Characterization of catalysts from item 7													
9. Testing stability of catalysts compare between catalyst with and without promoter (the best promoter)													
10. Result analysis, discussion and conclusion													

CHAPTER 2

THEORY AND LITERATURE REVIEWS

2.1 Ethyl lactate

Ethyl lactate or lactic acid ethyl ester is one of the organic compounds. The chemical formula of ethyl lactate that its molecular structure presents in **Figure 1**. It appears as colorless to light transparent liquid with rum. It is simply soluble in ethanol and other organic solvents. Ethyl lactate is the interesting green solvent from fermentation process of corn or carbohydrate. The special properties of ethyl lactate is a biodegradable, non-carcinogenic, an efficient and environmentally friendly solvent, non-volatile and non-ozone depleting. Ethyl lactate is manufactured from acid catalyzed esterification reaction between lactic acid and ethanol [3, 8]. Ethyl lactate is mostly used for the coatings industry as a result of its has the properties are high boiling point, high solvency, low vapor pressure, low surface tension and a specifically devoted solvent. In addition, ethyl lactate is a common solvent in industries including cosmetic, medicinal, food, coatings, paint and perfume production [9]. The ethyl lactate properties are show in **Table 1**.

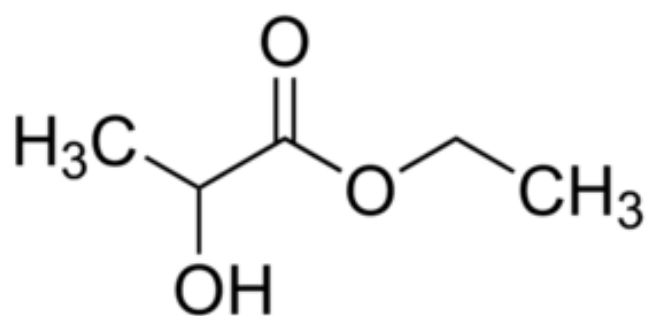



Figure 1 Chemical formula of ethyl lactate [10]

Table 1 Properties of ethyl lactate

Properties	Description
IUPAC name	Ethyl 2-hydroxypropanoate
Chemical formula	$\text{CH}_3\text{CH}(\text{OH})\text{CO}_2\text{CH}_2\text{CH}_3$
Molecular weight	118.13 g/mole
Density	1.03 g/cm ³
Boiling point	154 °C
Melting point	-25 °C
Appearance	Colorless to light transparent liquid
Solubility	Miscible with water (with partial decomposition), ethanol (95%), ether, esters, and hydrocarbons.
NFPA 704	

2.2 Lactic acid

Lactic acid is an important organic acid used in the industries including pharmaceutical, cosmetic, food and textile. The $\text{C}_3\text{H}_6\text{O}_3$ or $\text{C}_2\text{H}_4\text{OHCOOH}$ is chemical formula. Lactic acid is commercially manufacturing by fermentation process from sugars such as glucose derived from starch. It is used as a food acidifier to produce a sour taste and used as preservatives to prevent deterioration of food. In the petrochemical industry, refined lactic acid is often used a raw material for the production of biodegradable plastic, that is Polylactic acid, PLA [11-13]. There are two types of isomer such as D-isomer type and L-isomer type are shown in **Figure 2**. There are enantiomer and different of optical active, which has same chemical formula but different of 3 dimensions geometry [13] The lactic acid properties are present in **Table 2**.

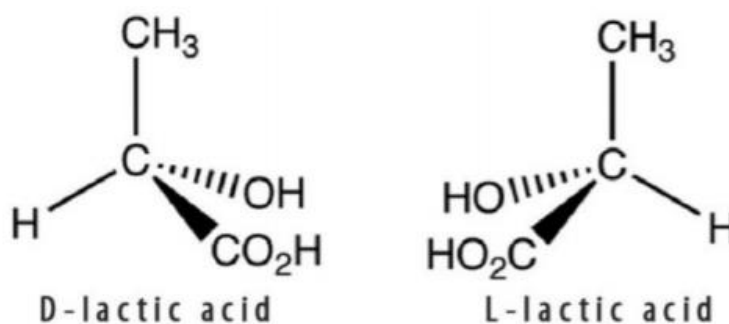



Figure 2 Structures of lactic acid [10]

Table 2 Properties of lactic acid

Properties	Description
IUPAC name	2-hydroxypropanoic acid
Chemical formula	$C_2H_4OHCOOH$
Molecular weight	90.08 g/mole
Density	1.206 g/cm^3
Boiling point	$122 \text{ }^\circ\text{C}$
Melting point	$18 \text{ }^\circ\text{C}$
Appearance	Colorless to light yellow transparent liquid
Solubility	Miscible with water
NFPA 704	

2.3 Esterification of ethyl lactate

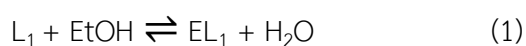
Esterification is the mechanism reaction in which two reactants include of alcohol and carboxylic acid form an ester as the reaction product. The catalytic esterification of ethanol and lactic acid using acid catalyst to perform ethyl lactate which is the important product for the chemical industry. The ethyl lactate esterification reaction that occurs is a reversible reaction. Ethyl lactate is the main product and water is the side product, which is the byproduct for this reaction (eq.1).

This includes adverse reactions to oligomers, esterification, and transesterification of oligomers (eq.2-eq.7) [3, 10]

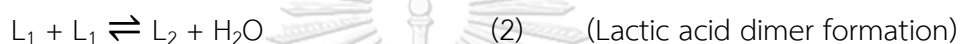
The production of ethyl lactate has traditionally been based on the esterification of ethanol and lactic acid, according to the reactions as followed equation (1-7) [3].

Note: Ethanol (EtOH) / Lactic acid (L_n) / Ethyl Lactate (EL_n) / Water (H_2O)

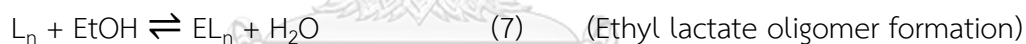
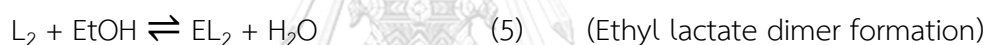
Main reaction



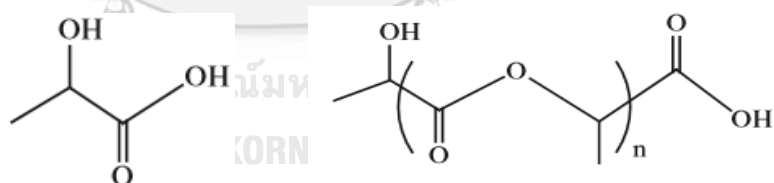
Side reaction



with $n \geq 2$

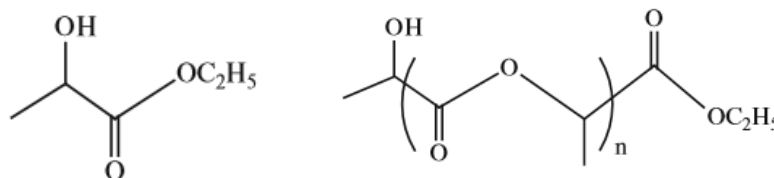


Where:



a) Lactic acid

b) Lactic acid oligomers



c) Ethyl lactate

d) Ethyl lactate oligomers (EL_{n+1})

Figure 3 Chemical formula of substance in system a) Lactic acid (L_1), b) Lactic acid oligomers (L_{n+1}), c) Ethyl lactate (EL_1), d) Ethyl lactate oligomers (EL_{n+1}) [3, 10]

2.4 Amberlyst-15

Amberlyst-15 is heterogeneous catalyst, it is a good and selective acid catalyst for esterification reactions. The current noticeable in synthetic applications of Amberlyst-15 catalyst [14]. Amberberlyst-15 is getting more attention because of its very beneficial acidic properties. It is also environmentally friendly. It is easy to buy as it is commercially available.[15]. For the structure of Amberlyst-15 is shown in **Figure 4**. The Amberlyst-15 properties are present in **Table 3**.

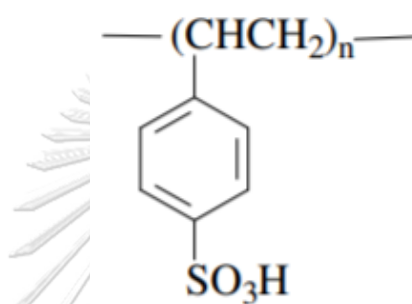


Figure 4 Structures of Amberlyst-15 [14]

Table 3 Properties of Amberlyst-15

Properties	Description
IUPAC name	1,2-bis(ethynyl) benzene; 2-ethenylbenzenesulfonic acid
Type	Strong acid
Structure	Macro reticular
Functional group	Sulfonic (SO_3H)
Chemical formula	$C_{18}H_{18}O_3S$ (isomer)
Molecular weight	314.40 g/mole
Bulk density	0.600 g/cm ³
Polymer density	1.410 g/cm ³
Internal porosity	0.36
Cross-linking degree	20 %
Particle size	0.35 to 1.2 mm
Average pore diameter	300 Å
Total pore volume	0.40 mL/g
Boiling point	516.7 °C at 760 mmHg

Properties	Description
Appearance	Brown-grey solid
Solubility	Insoluble in water

2.5 Montmorillonite clay (MMT catalyst)

Montmorillonite clay (MMT) is consist of stacked layers are two O-Si-O tetrahedral sheets sandwiching and connect with O-Al(Mg)-O octahedral sheet. It is a phyllosilicate mineral with nanolayered structure. Due to the isomorphous superseding, the layer is positively charged and then cations are subsist in the interlayered space of Mt. Neighboring layers. In addition, they are also held together primarily by van der Waals force and electrostatic force to form the primary particles of Mt. The particles then collect to form secondary micrometer-scale to millimeter-scale particles [16, 17] and the structure of montmorillonite clay as present in **Figure 5**.

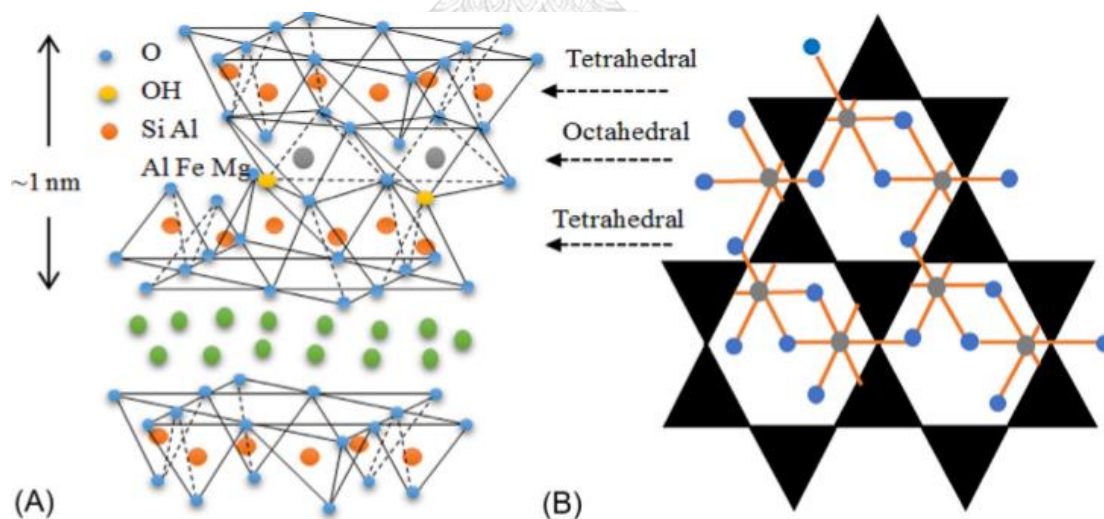


Figure 5 The structure of montmorillonite clay (A) Side view and (B) Top view of MMT [16]

2.6 Ammonium metatungstate (AMT)

Ammonium metatungstate (AMT) has the formula is $(\text{NH}_4)_6[\text{H}_2\text{W}_{12}\text{O}_{40}] \cdot n\text{H}_2\text{O}$ is a polycondensation product of ammonium tungstate solutions. At temperature found

that It has a very high solubility. The metatungstate ion or $[H_2W_{12}O_{40}]^{6-}$ is a polyoxometalate ion that forms in solution of monotungstate on pH adjustment. It is also known as dodecatungstate, which is Keggin-type polyoxometalate of the isopoly category; they are also known as heteropoly compounds, and in older literature as $m-WO_3$, hence naming metatungstate. The metatungstate ion has been popularly used commercially for 40 years [18]. The interesting redox properties of metatungstate have present feasible further applications in catalysis. The metatungstate ion and its especial solution properties are also a key to the technology of refining of tungsten from primary and secondary sources. For the catalyst application is extremely advertent, since structure properties are a key to understand the efficiency and stability of a catalyst [18, 19]. The ammonium metatungstate properties are present in **Table 4**.

Table 4 Properties of ammonium metatungstate

Properties	Description
Formula	$(NH_4)_6H_2W_{12}O_{40} \cdot xH_2O$
Compound formula	$H_{26}N_6O_{40}W_{12}$
Molecular weight	2956.3 g/mole
Melting point	100 °C
Appearance	Beige powder
Solubility	Miscible with water

2.7 Tungsten trioxide

Tungsten trioxide or WO_3 is a chemical compound including the transition metal tungsten and oxygen. It is received as an moderate in the recovery of tungsten from its minerals. Tungsten ores are treated with alkalis to produce WO_3 . Further reaction with carbon or hydrogen gas reduces tungsten trioxide to the tungsten metal. The tungsten trioxide properties are presented in **Table 5**.

Table 5 Properties of tungsten trioxide

Properties	Description
IUPAC name	Tungsten trioxide
Chemical formula	WO ₃
Molecular weight	231.84 g/mole
Density	7.16 g/cm ³
Boiling point	1,700 °C approximation
Melting point	1,473 °C
Appearance	Canary yellow powder
Solubility	Slightly soluble in HF, insoluble in water

2.8 Promoter

Promoter, substance added to a solid catalyst to improve its efficiency in a chemical reaction. Some promoters interact with active components of catalysts and thereby alter their chemical effect on the catalyzed substance. The interaction may cause changes in the electronic or crystal structures of the active solid component. A promoter is added in a few quantities to increase or maintain textures or increase a catalytic activity.

Chemical promoters improve the effectiveness of the catalyst often by permutation the electron distribution at the surface. Structural promoters help protect sintering and improve the mechanical properties. It is also possible that the catalyst and the promoter form a loose type of compound and this compound proffers a better chemisorption site for the reacting molecules. This may roughly describe the selectivity of the promoter action. It may also be possible that the catalyst-promoter pair offers competitive sites for adsorption to the molecules and the different atoms of the reacting molecules are chemisorbed on both the surfaces leaving the adsorbed molecules in a highly strained active form, thus supporting the reaction rate.

2.8.1 Zirconium (IV) oxynitrate hydrate

The chemical and physical properties of zirconia based catalysts make them attractive catalysts which can compete with zeolites, clays and oxides in industry [20]. The zirconium (IV) oxynitrate hydrate properties are presented in **Table 6**.

Table 6 Properties of Zirconium (IV) oxynitrate hydrate

Properties	Description
IUPAC name	Oxozirconium (2+); dinitrate; hydrate
Chemical name	Zirconyl nitrate hydrate
Molecular formula	$ZrO(NO_3)_2 \cdot xH_2O$
Molecular weight	231.23 g/mole
Appearance	White powder
Solubility	Soluble in alcohol

2.8.2 Platinum (II) acetylacetonate

Supported platinum-based catalysts are popularly used in chemical industries. Platinum is an effective catalyst in the dehydrogenation of alkanes when dispersed on high-surface area supports [21]. The platinum (II) acetylacetonate properties are presented in **Table 7**.

Table 7 Properties of Platinum (II) acetylacetonate

Properties	Description
IUPAC name	(Z)-4-hydroxypent-3-en-2-one; platinum
Chemical name	2,4-Pentanedione platinum (II) derivative
Chemical formula	$C_{10}H_{14}O_4Pt$
Molecular weight	393.29 g/mole
Density	2.362 g/cm^3
Melting point	$239.4 \text{ }^\circ\text{C}$
Appearance	Yellow solid
Solubility	Insoluble in water

2.9 Literature reviews

This chapter was reviewed for investigation of the study on the W/MMT catalyst for the esterification of ethanol with lactic acid, which were appropriate in the temperature calcination, promoters for synthesis catalyst. In addition, it had been investigated for deactivation of catalysts montmorillonite clay for esterification reaction.

W. Yu et al. (2017) [22] who studied quantity of WO_x-loaded montmorillonite catalysts and acid-activated catalyst and their catalytic behaviors in glycerol dehydration. The acid activation of WO_x loaded on MMT influenced the strength and number of acid site arising from acid exchange. For the result found that the highest catalytic activity of reaction is 13.5% W/MMT catalyst. Thus, W/MMT is one of the candidate acid catalysts owing to be good at higher acidity, which might appropriate for esterification.

J. Ma et al. (2009) [23] investigated the effect of membrane casting solution recipe, reaction temperature, initial molar ratio of ethanol to lactic acid and catalyst loading amount on the process for pervaporation-assisted esterification of lactic acid with ethanol, catalyzed by Amberlyst-15 ion-exchange resin. It was found that the catalyst loading with the difference percent weight from 0.5 to 3 wt% which exhibited the reaction rate increases with the higher percentage weight of Amberlyst-15 with value of 2 wt%. The result found that the initial molar ratio of ethanol/lactic acid (reactant) is 3:1 and the temperature 80 °C were the best condition occur to high catalytic activity.

C. S. M. Pereira et al. (2008) [24] who examined the effect of Amberlyst-15 in esterification of ethanol with lactic acid (88 wt%) varies the initial molar ratio of reactants of 1.1-2.8, catalyst loading 1.2-3.9 wt%, and temperature from 50 to 90 °C. For the reaction use the methodology based on the UNIQUAC model was improved to assign the thermodynamic equilibrium constant since in the literature there is disapprobation concerning the temperature complementing of the thermodynamic equilibrium constant. A simplified Langmuir-Hinshelwood kinetic model was used to

predict the experimental data. The proposed kinetic parameters are the preexponential factor, $k_0 = 2.70 \times 10^7 \text{ mol}^{-1} \text{ g}^{-1} \text{ min}^{-1}$, rate law is $r = \frac{k_0 a_{\text{Eth}} a_{\text{La}} - a_{\text{ELaW}}/K}{(1 + K a_{\text{Eth}} + K a_{\text{W}})^2}$ and the activation energy, $E_a = 49.98 \text{ kJ/mol}$. The equilibrium reaction constant is $K = 19.35 \exp(-515.13/T)$ (K) with reaction enthalpy 4.28 kJ/mol .

D. E. Lopez et al. (2007) [25] who studied the esterification of acetic acid and methanol about the effect of calcination temperature (400-900 °C) for at reaction time 60 °C for liquid phase, 120 °C for gas phase, and the liquid-phase transesterification of triacetin with methanol on the tungstated zirconia in order to examine the catalytic properties. In this work, the result showed that the catalyst that presented the optimum catalytic activity at 800 °C of calcination, for selectivity poisoning of the potential catalytic centers represent that Brønsted sites played the important role in carrying out these reactions.

S. Ramu et al. (2004) [6] who examined the effect of method of the catalyst preparation from both co-precipitation and impregnation method, including the tungsten loading. Moreover, the calcination temperature from 400 to 900 °C were varied for the esterification in methanol and palmitic acid was investigated on zirconia supported tungsten oxide. In this work, the result showed the 400-500 °C (low) of temperature calcined catalysts exhibited the respectability of tetragonal phase of ZrO_2 , further increase in calcination temperature, which lead to increase formation of the stable monoclinic phase from the tetragonal phase.

According to J. Yu et al. (2008) [26] who studied effect of calcination temperatures on microstructures and photocatalytic activity of tungsten trioxide hollow microspheres. For the calcination temperature at 300, 400, 500, 600 and 700 °C. The evidence suggested that the increasing calcination temperatures, the average pore size and average crystallite size increased. In the other hand, BET specific surface areas decreased. For the result the highest photocatalytic activity is the un-calcined and at 300 °C calcined. The reduce of specific surface areas at 400 °C affect to photocatalytic activity decreased. The photocatalytic activity of the catalyst sample remarkably increased again owing to the junction effect of two phases at 500 °C.

H. Gao et al. (2014) [27] who reported the catalytic wet peroxide oxidation degradation of orange acid occur from the calcination temperature of 300, 400, 500, 600 and 700 °C. It might maintain a adapted montmorillonite clay and retain FeOOH as active sites in the clay. However, at above temperature 500 °C (high temperature) heating process might obstruct the interlayer structure. However, the heating at 500 °C with the molar ratio 4:6 of Fe/Ni and 6% loading of active metal presented better stronger stability among and catalytic behavior and all the prepared materials.

B. Jiang et al. (2016) [28] who investigated the effect of calcination temperature (varies temperature 600, 700 and 800 °C) and Ni loading for glycerol steam reforming. The results found that the best activity occur from the calcination temperature at 700 °C , which would increase the metal dispersion and reducibility due to favor the formation of Ni-Al alloy and conserve the lamellar structure.

F.J.P. Schott et al. (2009) [29] who studied the promoters loading of Pt and ZrO₂ on WO₃ support catalyst are developed and characterized by temperature-programmed desorption of H₂ (H₂-TPD), N₂-physisorption (BET) and power X-ray diffraction (PXRD). For the result high catalytic activity in reduction of NO_x by H₂ reaction occur from most active catalyst is a Pt load of 0.3 wt% (vary loading 0.1-0.5 wt%).

M.L. Hernandez-Pichardo et al. (2012) [30] who reported the catalyst for he hydroisomerization n-hexane of reaction. For the systems catalyst as Pt supported on tungstate zirconia (Pt/WZ). The characterization results found that advise that the presence of iron modifies the nanostructure of the WO_x species on the zirconia surface which in turn produces the generation of active Brønsted acid sites thus increasing the efficiency of the tungsten content to the highest catalytic activity.

From all the above literature review, it shows condition for operated esterification of ethanol with lactic acid. The W/MMT could be one of the candidate catalysts owing to its high acidity, which was needed for esterification reaction of ethanol and lactic acid to ethyl lactate. To the best of our knowledge, no work in the

literature has been yet reported on the use of W/MMT for esterification reaction with ethanol and lactic acid to ethyl lactate with batch reactor at 80°C for 4 h. Furthermore, the temperature of calcination for synthesis W/MMT possibly affects to either physical or chemical properties. Thus, this research will investigate this effect on W/MMT in order to optimize the catalytic activity with calcined temperature of 375, 475, and 575 °C. Consequently, the improvement of catalyst may be needed for higher catalytic activity, which reviewed with above literatures such as Zr and Pt (0.3 wt% both). This promoter can provide the higher acidity, which can facilitate the active site for more active in order to higher catalytic activity.



CHAPTER 3

EXPERIMENTAL

This chapter describes the detail of an experimental research including of synthesis of montmorillonite clay catalyst with tungsten loading by wetness impregnation method. And the remain part synthesis of montmorillonite clay catalyst with tungsten loading and addition metal promoter by sequential impregnation method. The catalyst characterization techniques such as powder X-ray diffraction (XRD), Fourier-transform infrared spectroscopy (FTIR), N₂ physisorption (BET), scanning electron microscopy (SEM) and energy dispersive X-ray spectroscopy (EDX), temperature-programmed desorption of ammonia (NH₃-TPD), X-ray photoelectron spectroscopy (XPS) and X-ray fluorescence (XRF) are explained. The catalyst screening up on esterification of ethanol and lactic acid is also given.

3.1 Materials

The detail of chemicals used in the catalyst preparation are represented as below in **Table 8**.

Table 8 The chemicals used in the catalyst preparation

Chemicals	Formula	Supplier
Montmorillonite clay (MMT)	$(\text{Na,Ca})_{0.33}(\text{Al,Mg})_2(\text{Si}_4\text{O}_{10})(\text{OH})_2 \cdot n\text{H}_2\text{O}$	Sigma-Aldrich
Ammonium metatungstate hydrate (99.99%metals)	$(\text{NH}_4)_6\text{H}_2\text{W}_{12}\text{O}_{40} \cdot x\text{H}_2\text{O}$	Sigma-Aldrich
Zirconium (IV) oxynitrate hydrate 99%	$\text{ZrO}(\text{NO}_3)_2 \cdot x\text{H}_2\text{O}$	Sigma-Aldrich
Platinum (II) acetylacetonate 97%	$\text{Pt}(\text{C}_5\text{H}_7\text{O}_2)_2$	Sigma-Aldrich
Amberlyst-15	$\text{C}_{18}\text{H}_{18}\text{O}_3\text{S}$	Sigma-Aldrich

3.2 Catalyst preparation

The synthetic process of tungsten supported on montmorillonite catalyst is described by J. Liewchalermwong [31] as follows. First, WO_3 (13.5 wt%) on montmorillonite catalyst was prepared by the incipient wetness impregnation method. Ammonium metatungstate hydrate was used of 0.00941 g and dissolved in 10 ml of de-ionized water. Next, the prepared solution was gradually dropped into 0.45 g of montmorillonite clay. After that, the prepared catalyst sample was dried for 12 h at 110 °C in oven and was calcined at 375, 475 and 575°C with the heating rate of 10°C per minute for 4 hours under nitrogen gas. Then, choose the best result of calcination temperature and load each promoter (0.3 wt% as Zr, Pt) by the incipient wetness impregnation after W finished. Zirconium (IV) oxynitrate hydrate was used of 0.038 g and dissolved in 10 ml of de-ionized water. Platinum (II) acetylacetonate was used of 0.0302 g and dissolved in 10 ml of de-ionized water. Next, the prepared catalyst sample was dried for 12 h at 110 °C in oven and was calcined at 375, 475 and 575°C with the heating rate of 10°C per minute for 4 hours under nitrogen gas. Finally, the catalyst was ready to use in the reaction test.

3.3 Catalyst characterization

3.3.1 Powder X-ray diffraction (XRD)

The SIEMENS D-5000 X-ray diffractometer was being utilized to measure the crystalline phase structure of supports and catalysts by use $\text{CuK}\alpha$ radiation ($\lambda = 1.54439 \text{ \AA}$). The XRD patterns of catalysts were examined at the rate of 2.4 min^{-1} in the range 2θ from 20 to 80 degrees with resolution of 0.02 degrees.

3.3.2 Fourier-transform infrared spectroscopy (FTIR)

Fourier-transform infrared spectroscopy (FTIR) using Vertex 70, Bruker, equipped with a mercury-cadmium-telluride (MCT) detector. It was used to examine specific structural characteristics of the chemical functional group.

3.3.3 N₂ physisorption (BET)

N₂ physisorption technique using a Micromeritics ASPS 2020 at liquid nitrogen temperature (−196°C). It was applied to measure specific surface area (calculated by the BET method), pore size distribution, pore diameter, average pore volume, (using the BJH desorption analysis) and adsorption/desorption isotherm.

3.3.4 Scanning electron microscope (SEM) and energy dispersive X-ray spectroscopy (EDX)

Scanning electron microscope (SEM) using a model of JEOL mode JSM-6400 and EDX using Link Isis series 300 program. And energy dispersive X-ray spectroscopy (EDX) were employed to assign the morphology and examined the elemental distribution of catalysts.

3.3.5 Temperature-programmed desorption of ammonia (NH₃-TPD)

Temperature-programmed desorption of ammonia (NH₃-TPD) was used for analyzed the total amount of acid sites of all the catalysts using a Micromeritics Chemisorb 2750. Firstly, 0.03 g of quartz wool and 0.05-0.1 g of catalyst were packed in a glass tube and then pretreated with helium flow of 25 mL/min at 200°C for 1 h. After that, the catalyst sample was adsorbed 15% of NH₃/He at room temperature for 1 h. Finally, the chemisorbed NH₃ was desorbed under a He flow from 30 to 500 °C. Moreover, it was held at 500 °C for 1 h. The amount of ammonia in effluent was determined by the thermal conductivity detector (TCD).

3.3.6 X-ray photoelectron spectroscopy (XPS)

X-ray photoelectron spectroscopy (XPS) using MgK α X-ray radiation (1253.6 eV) and AlK α X-ray radiation (1486.6 eV) at voltage 15 kV and current of 12 mA. It was applied to determine the binding energy of each axis atomic orbital in the catalysts. And the catalyst was pretreated in the oven at 110°C overnight before the analysis process.

3.3.7 X-ray fluorescence (XRF)

X-ray fluorescence (XRF) was a technique for analyzing the type of element and the trace elements in a sample. Based on the principle that electrons in atomic orbits change a high-energy class to a lower-energy class and emit energy in the form of X-rays of a specific energy (characteristic X-ray) of each element.

3.4 Catalytic activities and stabilities

3.4.1 Calibration of reactants, products

The detail of chemicals used in the preparation is represented in **Table 9**.

Table 9 The chemicals used in the calibration of reactants and product

Chemicals	Formula	Supplier
>98 wt% Ethyl lactate	$C_5H_{10}O_3$	TCI
99 wt% Ethanol	C_2H_5OH	Merch
90 wt% Lactic acid	$CH_3CHOHCOOH$	KOSDAQ

3.4.2 Esterification reaction of ethanol with lactic acid

The esterification reaction of ethanol with lactic acid was operated in batch reactor (a 3-neck round bottomed flask soaking in a silicone oil bath). The molar ratio of reactants are ethanol/lactic acid at 3:1 was added into the flask, followed by adding of catalyst (at 2 wt% of lactic acid) into the reactant mixture while stirring at 700 rpm. Next, the mixture was heated to 80°C and kept it at this temperature for 4 h. After that, cooling down to room temperature, the products and the catalyst were separated by filtration. For the catalyst after filtration take it to dry by oven 110 C for 4 h.

The catalytic stability was investigated by reusing the chosen catalysts in the identical reaction test as mentioned above for 3 times (cycles). In each cycle, the spent catalyst was filtered and dried at 110 °C in oven for 4 hours prior to start the next cycle of reaction test.

Shimadzu gas chromatography was used to analyze product distribution with flame ionization detector (GC-FID) using capillary column (DB-5) at 150°C. The

operating condition of GC is present in **Table 10** and flow chart of esterification reaction of ethanol with lactic acid is shown in **Figure 6**.

Table 10 The operating condition of gas chromatography (GC)

Gas chromatograph	Shimadzu GC 14-A
Detector	FID
Capillary column	DB-5
Carrier gas	Hydrogen gas, Nitrogen gas
Column temperature	Initial 40 °C Final 40 °C
Injector temperature	150 °C
Detector temperature	150 °C
Time analysis	8 min

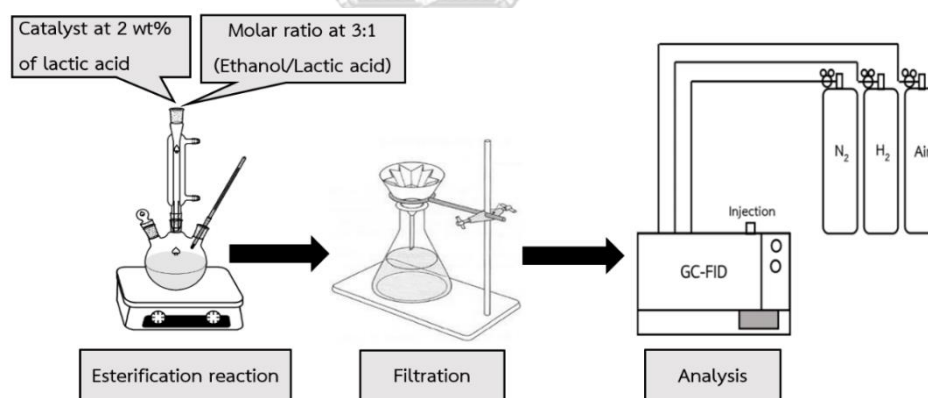


Figure 6 Flow chart of esterification reaction of ethanol with lactic acid

3.4.3 Analysis and calculation

The catalytic activities in esterification of ethanol and lactic acid can be measured from lactic acid conversion, product selectivity and ethyl lactate yield with equations as follows;

$$\text{Conversion (\%)} = \frac{\text{Lactic acid in} - \text{Lactic acid out}}{\text{Lactic acid in}} \times 100$$

$$\text{Selectivity (\%)} = \frac{\text{Ethyl lactate}}{\text{All product}} \times 100$$

$$\text{Ester yield (\%)} = \frac{\text{molar ester produced}}{\text{molar acid added}} \times 100 \text{ or } \frac{\text{Conversion} \times \text{Selectivity}}{100}$$



CHAPTER 4

RESULT AND DISCUSSION

This chapter was to describe the results and discussion on the characteristic properties, catalytic activities and stability of different catalysts in esterification of ethyl lactate via ethanol and lactic acid. It was divided into three parts. The first part and second parts explained characteristic properties and catalytic activities in esterification of W supported on montmorillonite (MMT) with various calcination temperatures (375, 475, 575 °C) and the selection the best calcination temperature for the suitable promoter selection (Zr, Pt) was chosen. The final part focused on the comparison of result from the first and second parts to study of stability of catalysts between the best result in each part with the commercial Amberlyst-15 catalyst on esterification via ethanol and lactic acid using synthesized catalysts, which gave the highest lactic acid conversion or ethyl lactate yield.

4.1 The optimal calcination temperature selection

4.1.1 Catalyst characterization

4.1.1.1 X-ray Powder Diffraction (XRD)

The X-ray diffraction (XRD) patterns of MMT and W/MMT calcined at 375, 475 and 575 °C catalysts are shown in **Figure 7**. As seen, both MMT and W/MMT presented the diffraction peaks located at 2θ degrees of 21°, 28° and 35° representing the characteristic peaks of montmorillonite clay [32]. For all W/MMT catalysts, they exhibited main peaks located at 2θ degrees of 26.6°, 36.8°, 50° and 60° showing the characteristic peaks of hexagonal-WO₃ [33].

In addition, it was found that W/MMT 375 exhibited the XRD peaks located at 2θ degrees of 43.2° and 46.3°. These peaks revealed the presence of monoclinic-WO₃, whereas, W/MMT 475 exhibited the XRD peaks located at 2θ degrees of 23.9°, 43.2°. For W/MMT 575, it was found only one peak located at 2θ degrees of 23.9° indicating the characteristic peak of monoclinic-WO₃ [33, 34].

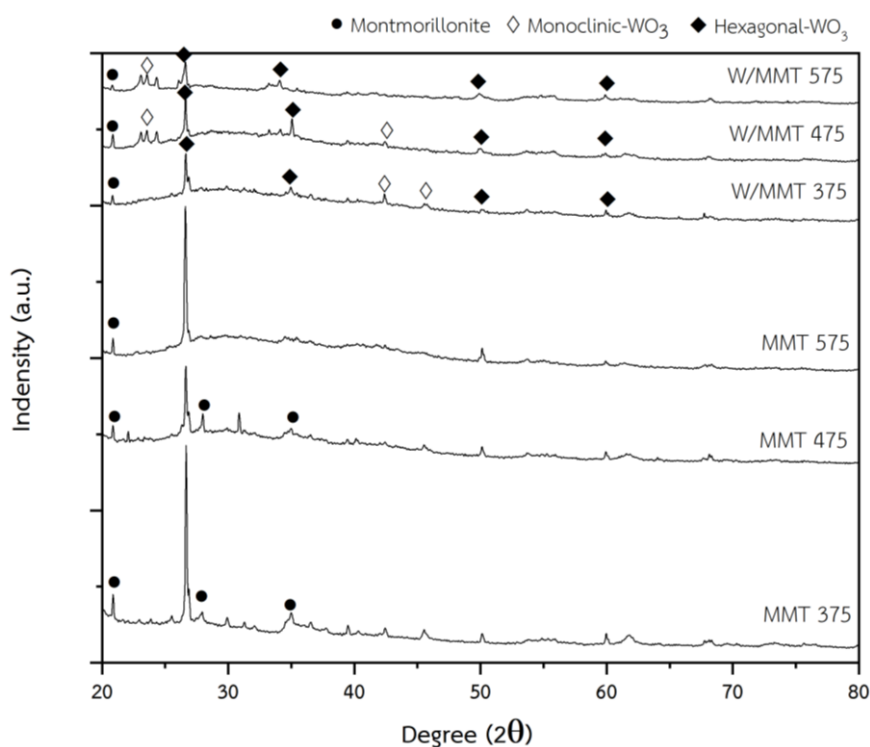


Figure 7 X-ray powder diffraction patterns of various MMT and W/MMT catalysts calcined at different temperatures

4.1.1.2 Fourier-transform infrared spectroscopy (FTIR)

The Fourier-transform infrared spectroscopy (FTIR) spectra at wavenumber range of 500 nm^{-1} to 400 nm^{-1} of all MMT catalysts and W/MMT catalysts are presented in **Figure 8** and the according band assignments are concluded in **Table 11**. It revealed that all catalysts indicated the absorption bands at 585.1 , 577.8 , 568.3 , 586.4 , 584.4 and 574.1 cm^{-1} , which were assigned to the Al-O-Si bending vibration [35]. The peak at 798.7 , 799.8 , 798.8 , 796.0 , 798.3 and 797.0 cm^{-1} were assigned to Al-Mg-OH [36]. In addition, the peak at 1622.3 , 1619.4 and 1616.3 cm^{-1} were found only in the W/MMT catalyst corresponding to W-OH planes [37]. The characteristic IR bands of MMT 575 and W/MMT 375 catalysts particularly occurred at 1738.6 and 1739.7 cm^{-1} corresponding to H-O-H bending [36]. Consequently, the W/MMT catalyst was found to have the functional groups of W (W-OH) corresponding with the XRD result.

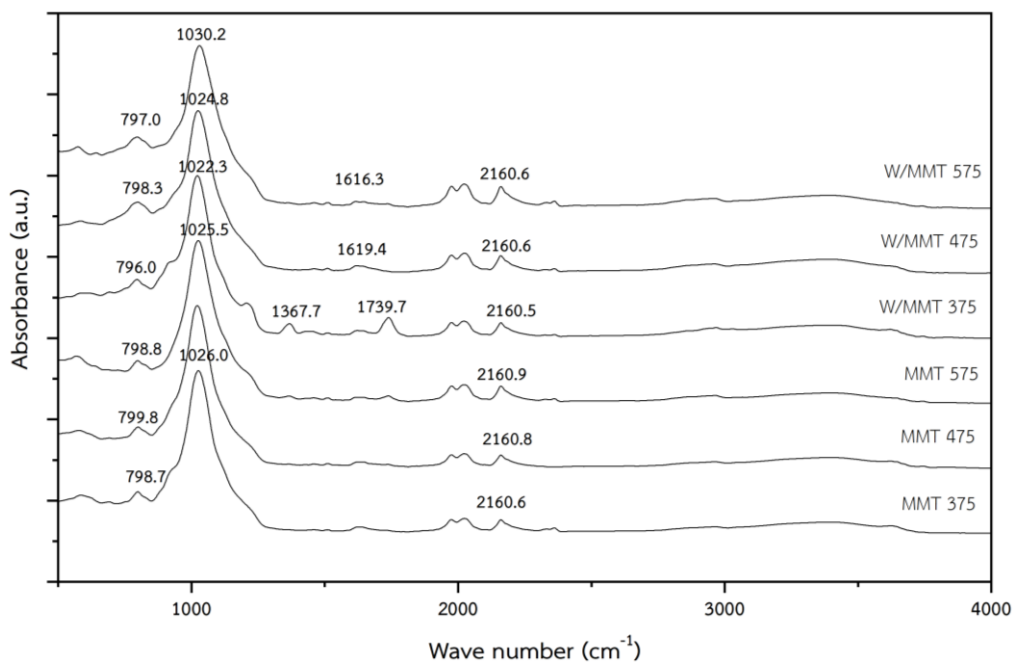


Figure 8 FTIR spectra of MMT and W/MMT catalysts

Table 11 FTIR assignments according to wavenumber (cm^{-1}) of MMT and W/MMT catalysts

MMT 375	MMT 475	MMT 575	W/MMT 375	W/MMT 475	W/MMT 575	Assignments
585.1	577.8	568.3	586.4	584.4	574.1	Al-O-Si
798.7	799.8	798.8	796.0	798.3	797.0	Al-Mg-OH
1026.0	1021.7	1025.5	1022.3	1024.8	1030.2	Si-O
			1206.3			Si-O
			1367.7			Si-O
			1622.3	1619.4	1616.3	W-OH
		1738.6	1739.7			H-O-H
		2964.3	2969.0	2960.9	2961.0	-OH stretching
3387.6	3391.5	3396.0	3391.4	3382.8	3385.1	-OH stretching

4.1.1.3 N₂ physisorption (BET)

The BET surface area, pore volume, pore diameter and adsorption/desorption isotherm of MMT and W/MMT catalysts were determined by N₂-physisorption, and the results are presented in **Table 12**. It was found that the BET surface area and pore volume decreased after W loading on MMT and W/MMT 575 (the highest calcination temperature) exhibited the lowest BET surface area among other catalysts. However, after W loading on MMT, all catalysts showed the decrease in surface area and pore volume due to some pore blockage caused by W loading [38].

Table 12 Properties of MMT and W/MMT catalysts

Catalyst	BET surface area ^a (m ² /g)	Pore volume ^b (cm ³ /g)	Pore diameter ^b (nm)
MMT 375	183	0.30	4.5
MMT 475	185	0.33	4.6
MMT 575	200	0.32	4.6
W/MMT 375	114	0.19	4.7
W/MMT 475	110	0.20	5.4
W/MMT 575	95	0.18	5.3

^a Determined from BET method ^b Determined from BJH desorption method

The adsorption/desorption isotherms indicating the pore structure of MMT 375, MMT 475, MMT 575, W/MMT 375, W/MMT 475 and W/MMT 575, which were analyzed by the N₂ adsorption-desorption isotherms are presented in **Figure 9** to **Figure 14**, respectively. For the MMT catalysts and W/MMT catalysts, they exhibited the type IV isotherm indicating the mesoporous structure with type H3 hysteresis loop according to IUPAC classification (International Union of Pure and Applied Chemistry) [39], and capillary condensation in the pores at relative pressure (P/P₀) approach 0.40. In addition, type IV isotherms are given by mesoporous adsorbents.

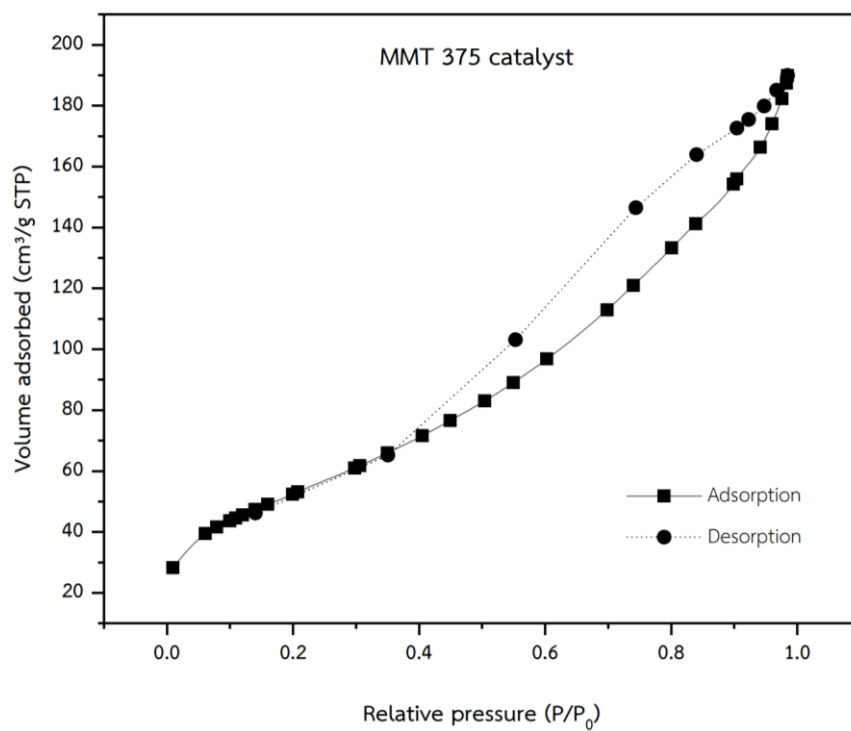


Figure 9 N_2 adsorption-desorption isotherm of MMT 375

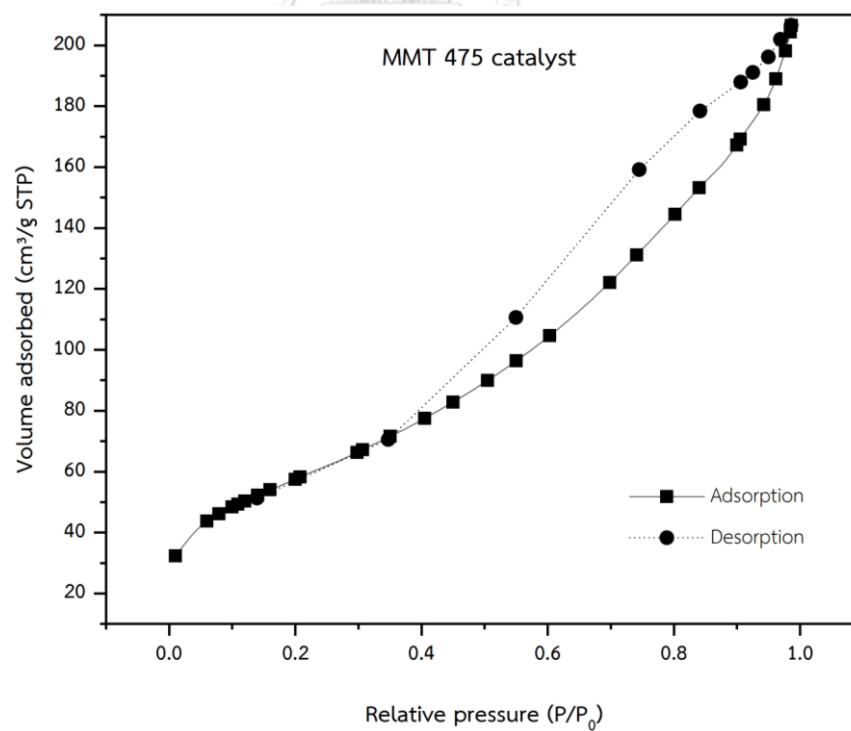


Figure 10 N_2 adsorption-desorption isotherm of MMT 475

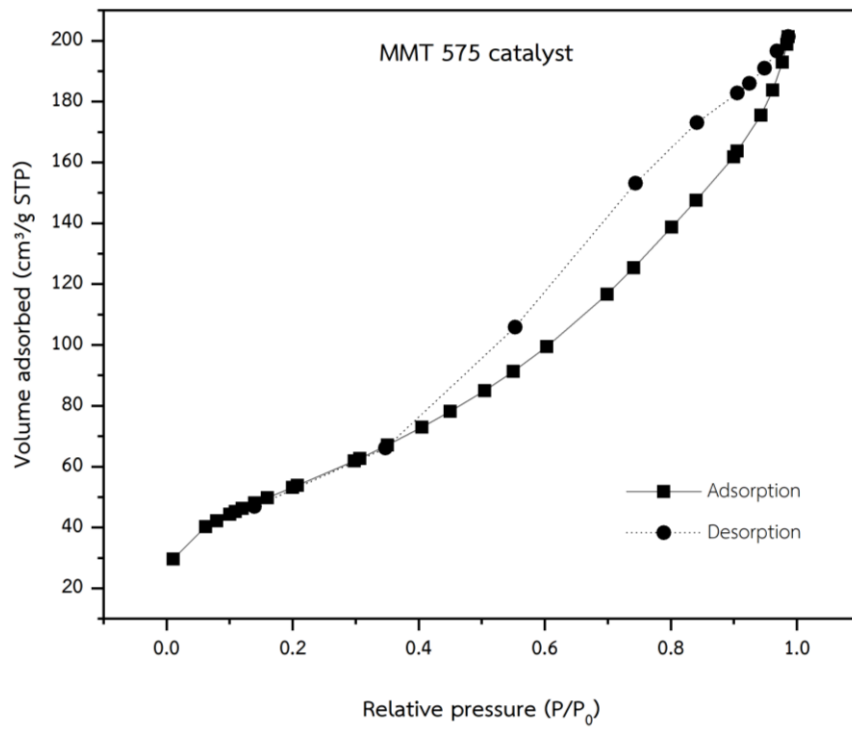


Figure 11 N₂ adsorption-desorption isotherm of MMT 575

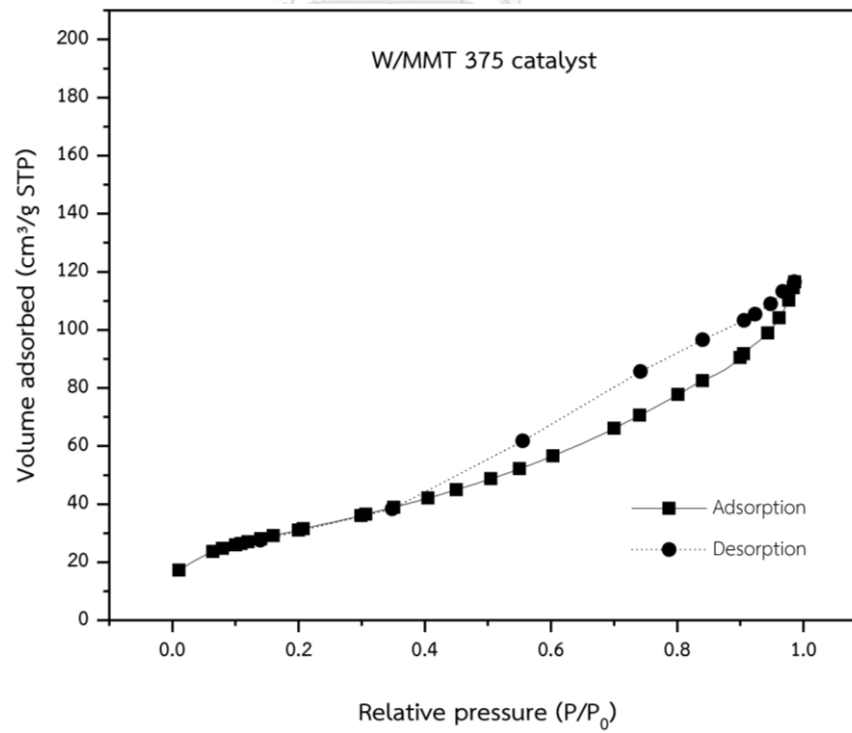


Figure 12 N₂ adsorption-desorption isotherm of W/MMT 375

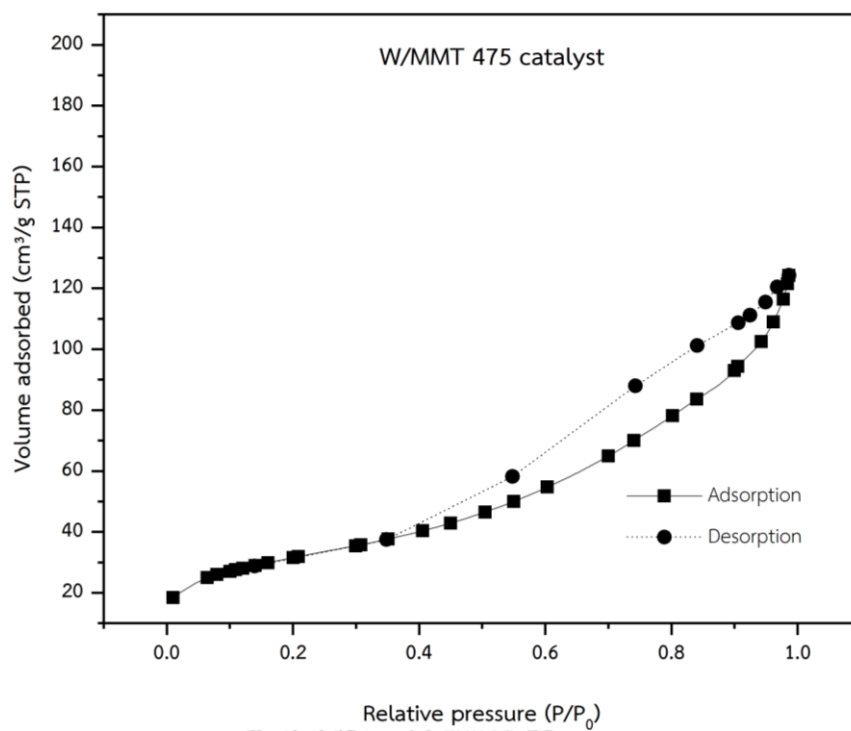


Figure 13 N₂ adsorption-desorption isotherm of W/MMT 475

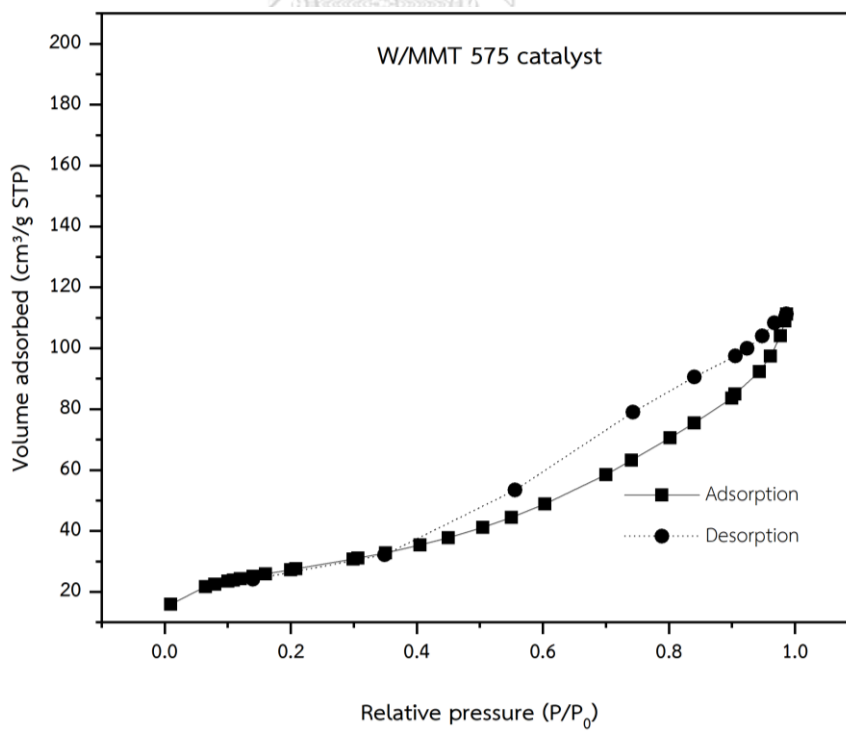


Figure 14 N₂ adsorption-desorption isotherm of W/MMT 575

4.1.1.4 Scanning electron microscope (SEM) and Energy dispersive X-ray spectroscopy (EDX)

The morphologies of all catalysts were analyzed by scanning electron microscope (SEM) as shown in **Figure 15**. For the **Figure 15(a)**, **Figure 15(b)** and **Figure 15(c)**, they are presented morphologies of MMT external surface indicating the irregular shapes and porous particles. However, after making the W supported on MMT catalysts calcined at different temperatures, their morphologies are shown in **Figure 15(d)**, **Figure 15(e)** and **Figure 15(f)**. It was found particles cover on surface area which are predicted to be W particles replaced the surface area and were distributed in the pores of MMT.

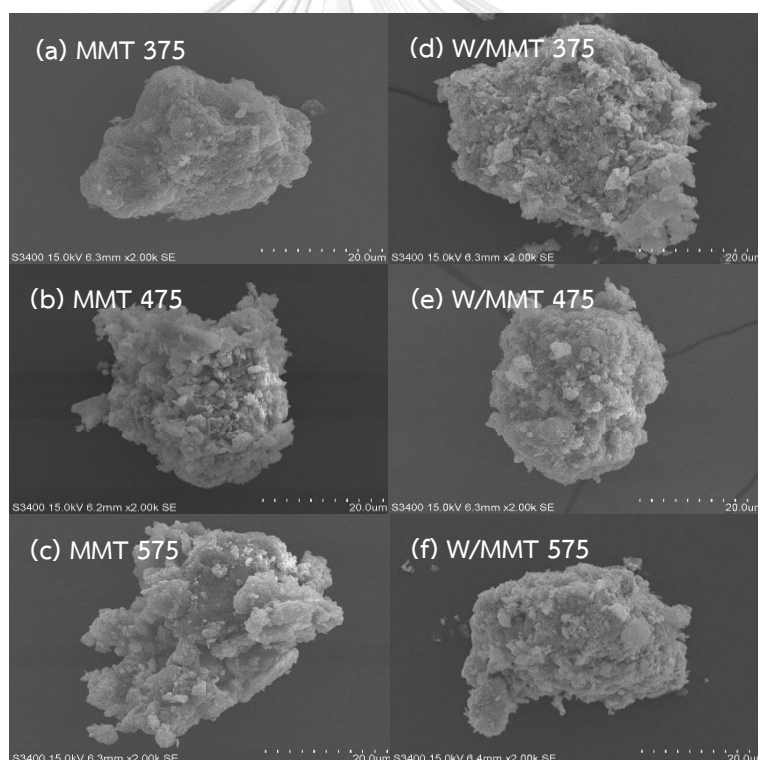


Figure 15 The morphologies of montmorillonite clays all temperature (MMT 375, MMT 475 and MMT 575) and tungsten supported on montmorillonite clays all temperature (W/MMT 375, W/MMT 475 and W/MMT 575) measured by SEM at mag.

X2,000

The elemental distribution of all catalysts can be quantitatively analyzed by energy dispersive X-ray spectroscopy (EDX) as shown in **Table 13**. It was found that % weight of elemental distribution for O as the major element can be observed along with other elements including N, Na, Si, Al and Ca for the MMT catalysts. For the W/MMT catalysts, the addition element distribution of W was found. The W/MMT 375 catalyst had the highest % weight of W (ca. 70%) distributed on the external surface.

Table 13 Elemental distribution of montmorillonite clays (MMT 375, MMT 475 and MMT 575) and W/MMT catalysts obtained by EDX

Catalyst	% Weight						
	N	O	Na	Si	Al	Ca	W
MMT 375	7.72	69.17	0.89	3.32	17.35	1.54	-
MMT 475	7.52	68.69	0.35	2.90	19.16	1.39	-
MMT 575	9.64	67.95	1	2.10	18.48	0.83	-
W/MMT 375	2.90	23.43	0.21	0.35	3.81	0.44	69.67
W/MMT 475	2.62	25.53	0.1	0.42	3.40	0.43	67.50
W/MMT 575	2.58	26.83	0.21	0.44	3.36	0.44	66.14

4.1.1.5 Temperature-programmed desorption of ammonia (NH₃-TPD)

Temperature-programmed desorption of ammonia was used to define the strength of acid site of all W/MMT catalysts measured by the desorption temperature of ammonia. For the results, the acid sites can be classified into two main groups including weak acid sites indicating the peak at temperature below 250 °C, and the peak observed at 250-400 °C relates to the moderate acid sites and more than 400 °C is assigned to the strong acid sites [40]. In addition, NH₃-TPD was examined to measure the surface acidity of all catalysts. The amount of acidity of all catalysts can be determined by integration of desorption peak area of ammonia according to the Gauss curve fitting method and presented in **Table 14**. It was found that W/MMT 475 catalyst exhibited the highest amount of moderate to strong acid sites and total acid sites among other catalysts. It revealed that W/MMT 575 catalyst exhibited the lowest

amount of moderate to strong acid sites and total acid sites. However, the commercial catalyst i.e. Amberlyst-15 was found to have the highest amount of acidity than all synthesized catalysts. The higher desorption temperature associated to the strong acid sites is commonly referred to the ammonia desorption from the Brønsted acid sites [41].

Table 14 The amount of acidity of tungsten supported on montmorillonite clays (W/MMT 375, W/MMT 475 and W/MMT 575) by NH₃-TPD compared with Amberlyst-15

Catalyst	Acidity (μmol NH ₃ /g)		
	Weak	Moderate to strong	Total acid site
W/MMT 375	392.1	905.5	1297.6
W/MMT 475	319.6	1279.2	1598.8
W/MMT 575	153.4	689.4	842.8
Amberlyst-15 ^a	551.5	3648.5	4200.0

^a V.L.C. Goncalves et al. (2008) who reported acidity of Amberlyst-15 [42].

4.1.1.6 X-ray photoelectron spectroscopy (XPS)

X-ray photoelectron spectroscopy was used to determine the surface properties of all catalysts. The Na 1s, O 1s, N 1s, Ca 2p, C 1s, Si 2p and Al 2p peak for the MMT catalysts and additional peak of W 4f1 and W 4f2 for the W/MMT catalysts are presented in **Table 15**. The Na 1s signal exhibited the highest binding energy around 1070 eV indicating Na⁺ ions in MMT [43]. The second one is the O 1s signal around 532.7-534.5 eV that can be assigned to lattice oxygen species [44]. Furthermore, the W/MMT catalyst revealed the W 4f1 and W 4f2 at 38 and 27 eV, respectively represented the WO₃ state (W⁶⁺) [45].

Table 15 XPS signals distribution of montmorillonite clays all temperature (MMT 375, MMT 475 and MMT 575) and tungsten supported on montmorillonite clays all temperature (W/MMT 375, W/MMT 475 and W/MMT 575)

Catalyst	Binding energy (eV)								
	Na	O	N	Ca	C	Si	Al	W	W
	1s	1s	1s	2p	1s	2p	2p	4f1	4f2
MMT 375	1070.2	534.0	395.5	347.5	285.0	103.3	76.4	-	-
MMT 475	1070.1	534.5	408.0	346.1	285.0	103.5	76.9	-	-
MMT 575	1073.5	534.2	405.4	352.4	285.0	103.9	76.7	-	-
W/MMT 375	1068.0	534.1	397.8	352.7	285.0	103.3	76.9	38.2	27.4
W/MMT 475	1080.9	534.1	397.2	347.5	285.0	102.8	77.0	38.7	26.9
W/MMT 575	1082.4	533.9	397.3	348.9	285.0	102.66	76.5	38.4	26.3

The surface compositions of all catalysts are presented in **Table 16**. It was found that the mass concentration (%) of the O 1s signal was the highest around 48-68 % among other elements. The W 4f1 and 4f2 signal had the mass concentration around 3-6 % on the catalyst surface.

Table 16 Surface compositions of montmorillonite clays all temperature (MMT 375, MMT 475 and MMT 575) and tungsten supported on montmorillonite clays all temperature (W/MMT 375, W/MMT 475 and W/MMT 575) by XPS

Catalyst	% Mass conc								
	Na	O	N	Ca	C	Si	Al	W	W
	1s	1s	1s	2p	1s	2p	2p	4f1	4f2
MMT 375	1.88	67.82	1.44	1.01	13.25	6.82	6.84	-	-
MMT 475	2.99	68.15	1.25	0.87	11.65	6.61	6.56	-	-
MMT 575	1.98	65.71	1.89	0.93	13.25	7.91	7.90	-	-
W/MMT 375	2.58	56.43	1.77	1.55	15.46	4.64	4.60	4.59	4.02
W/MMT 475	3.35	48.76	1.49	1.03	18.97	5.19	5.23	3.95	3.66
W/MMT 575	1.94	52.97	1.37	1.47	15.92	5.69	5.73	6.31	4.38

4.1.1.7 X-ray fluorescence (XRF)

X-ray fluorescence method was used to identify the major minerals and chemical compounds of the W/MMT catalysts as presented in **Table 17**. It was found that the element of W had the highest of concentration around 50-56% (according with EDX result) and the element of Si was around 29-33% in descending order. However, The SiO₂ had the highest concentration of the compound as 45-50% and WO₃ had the concentration around 33-39%. Therefore, the catalysts mainly consist of the SiO₂ and WO₃ compounds including the main concentrations of SiO₂ and WO₃, respectively.

Table 17 XRF analysis result of W/MMT catalysts

Analytical Element	Concentration (%)			Analytical Compound	Concentration (%)		
	W/MMT	W/MMT	W/MMT		W/MMT	W/MMT	W/MMT
	375	475	575		375	475	575
Na	0.204	0.195	0.213	Na ₂ O	0.233	0.226	0.246
Al	6.539	5.442	5.901	Al ₂ O ₃	9.343	7.948	8.601
Si	33.147	29.373	29.362	SiO ₂	49.711	45.291	45.181
K	2.818	2.486	2.806	K ₂ O	1.958	1.807	2.032
Ca	0.423	0.435	0.425	CaO	0.338	0.365	0.355
Ti	0.805	0.757	0.762	TiO ₂	0.761	0.751	0.753
Fe	5.813	5.406	5.318	Fe ₂ O ₃	4.587	4.494	4.401
W	50.25	55.904	55.214	WO ₃	33.069	39.118	38.432

4.1.2 Catalytic activities

The catalytic activities of the synthesized catalyst (W/MMT) were tested in esterification of ethanol and lactic acid and compared the result to the commercial catalyst Amberlyst-15. The yield of ethyl lactate for all catalysts is listed in **Figure 16**. It can be regard that the highest yield of ethyl lactate of 43.2% was obtained from W/MMT 375 catalyst, whereas the W/MMT 475 and W/MMT 575 catalysts exhibited the ethyl lactate yields of 37.3 and 33.3%, respectively. However, the highest yield of ethyl

lactate was found at 57.8%, which was obtained from the commercial catalyst Amberlyst-15. Based on NH_3 temperature-programmed desorption, it indicated that the Amberlyst-15 catalyst had the highest acidity, which is related to the highest conversion as well.

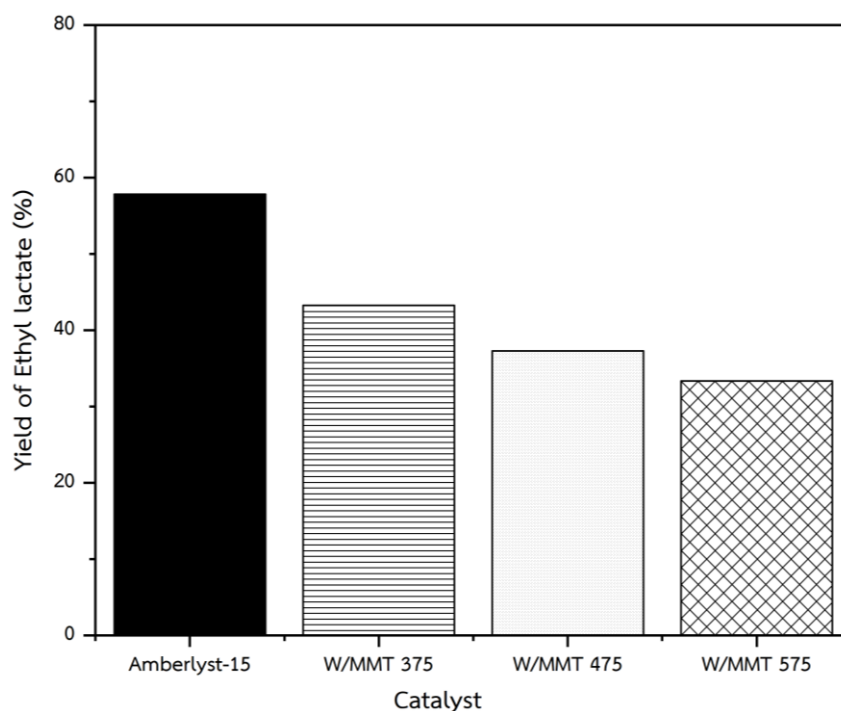


Figure 16 comparison of ethyl lactate conversion between Amberlyst-15 with W/MMT catalysts calcined at different temperatures (375, 475 and 575 °C)

4.1.3 Summary

After the reaction test of tungsten supported on montmorillonite clay (W/MMT) catalysts calcined at different temperatures including 375, 475 and 575 °C, the catalyst that provided the highest ethyl lactate yield was chosen for further study. Based on the characterization studies, it revealed that the W/MMT475 catalyst exhibited the highest acidity, followed by W/MMT375 and W/MMT575, respectively. However, from the surface area result, W/MMT375 exhibited the highest surface area, followed by W/MMT475 and W/MMT575, respectively. When all catalysts were tested in esterification of ethanol and lactic acid, it revealed that the W/MMT375 catalyst was

found to have the highest yield of ethyl lactate around 43.2 %. Therefore, for the conclusion of this part the W/MMT catalyst calcined at 375 °C (W/MMT 375 catalyst) was chosen for further study of effect of promoters.

4.2 The suitable promoter selection

4.2.1 Catalyst characterization

4.2.1.1 X-ray Powder Diffraction (XRD)

The X-ray diffraction (XRD) patterns of W-Zr/MMT and W/MMT calcined at 375°C denoted as W-Zr/MMT 375 and W-Pt/MMT 375 catalysts are shown in **Figure 17**. For the W-Zr/MMT 375 catalyst, it presented the diffraction peaks located at 2θ degrees of 28.3°, 31.5°, 35.5° and 40.9° indicating the characteristic peak of monoclinic- ZrO_2 , and at 2θ degrees of 36.1° and 50° showing the characteristic peak of tetragonal- WO_3 [46]. It was found that the characteristic peak of monoclinic- WO_3 was stronger than hexagonal- WO_3 , which is different from the W-Pt/MMT 375 showing that the characteristic peaks of hexagonal- WO_3 was stronger. The W-Pt/MMT 375 exhibited XRD peaks located at 2θ degrees of 39°, 46° and 68° indicating the characteristic peaks of Pt [47].

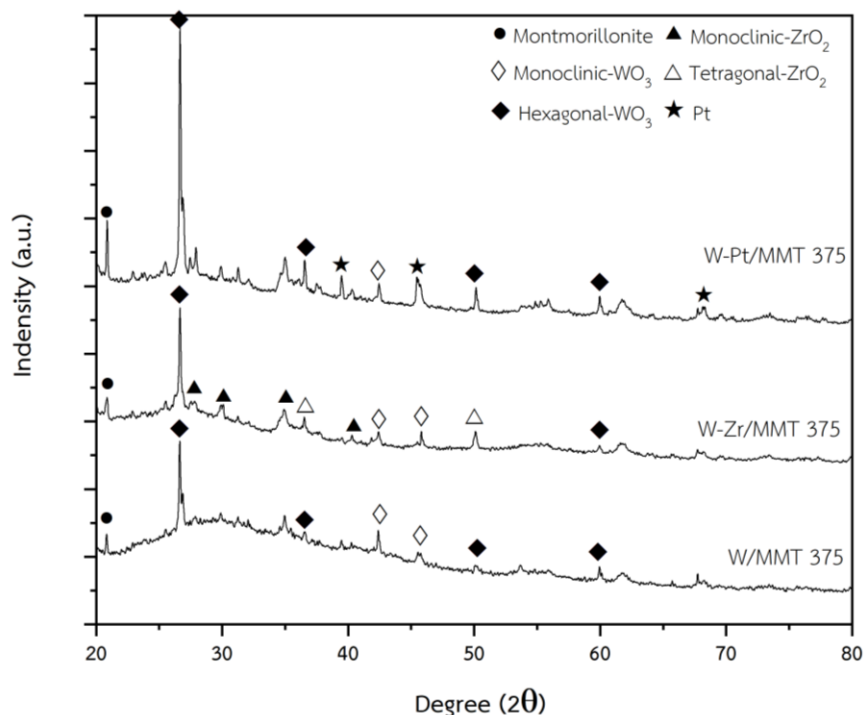


Figure 17 XRD patterns of the W-Zr/MMT 375 and W-Pt/MMT 375 catalysts

4.2.1.2 Fourier-transform infrared spectroscopy (FTIR)

The Fourier-transform infrared spectroscopy (FTIR) spectra at wavenumber range of 500 cm^{-1} to 400 cm^{-1} of W-Zr/MMT 375 and W-Pt/MMT 375 catalysts are shown in **Figure 18** and the according band assignments are concluded in **Table 18**. It was found that of the W-Pt/MMT 375 catalyst revealed the absorption band at 2035.6 cm^{-1} , which was assigned to the Pt-Pt bond stretching [48]. For the W-Zr/MMT 375 catalyst, it exhibited the peak at 2880.4 cm^{-1} , which was assigned to Zr-O-W [49]. Consequently, the W-Zr/MMT 375 and W-Pt/MMT 375 catalysts were found to have the functional groups of Zr (Zr-O-W) and Pt (Pt-Pt stretching) corresponding with the XRD result.

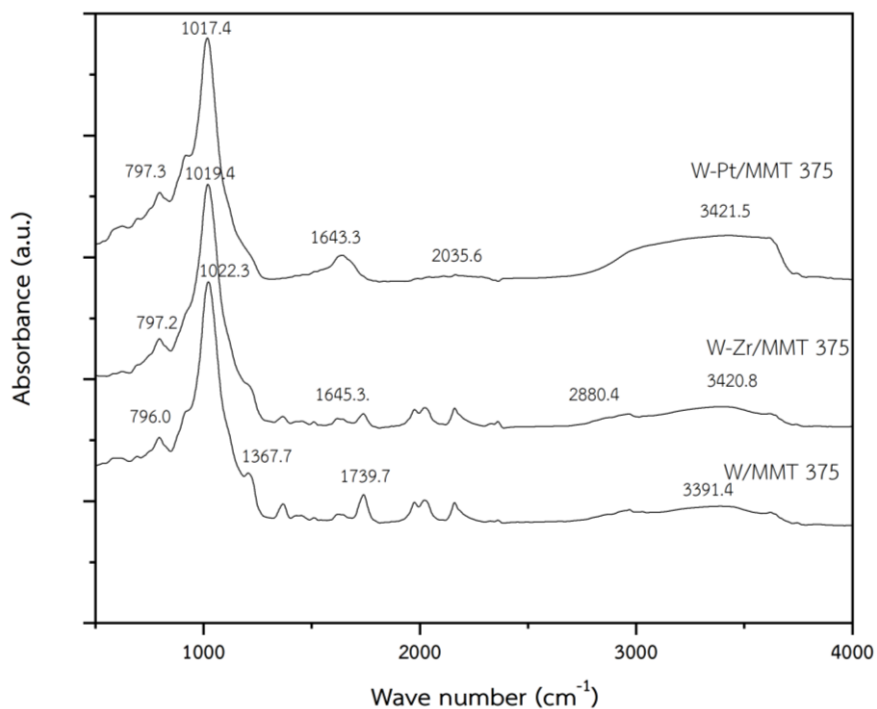


Figure 18 FTIR spectra of W/MMT 375, W-Zr/MMT 375 and W-Pt/MMT 375 catalysts

Table 18 FTIR assignments of W/MMT 375, W-Zr/MMT 375 and W-Pt/MMT 375

W/MMT 375	W-Zr/MMT 375	W-Pt/MMT 375	Assignments
586.4			Al-O-Si
796.0	797.2	797.3	Al-Mg-OH
1024.8	1022.3	1017.4	Si-O
1691.4	1645.3	1643.3	W-OH
		2035.6	Pt-Pt stretching
	2880.4		Zr-O-W
2960.9			-OH stretching
3382.8	3420.8	3421.5	-OH stretching

4.2.1.3 N₂ physisorption (BET)

The BET surface area, pore volume, pore diameter and adsorption/desorption isotherm of the W-Zr/MMT 375 and W-Pt/MMT 375 catalysts were determined by N₂-

physisorption, and the results of both promoted catalysts compared with the W/MMT 375 catalyst are presented in **Table 19**. It was found that the BET surface area and pore volume of W-Zr/MMT 375 catalyst decreased and exhibited the lowest BET surface area after Zr loading on W/MMT 375. This is because of the blockage of pore caused by Zr promoter [38]. However, the W-Pt/MMT 375 exhibited increased BET surface area and pore volume perhaps due to the increase dispersion of W by Pt promoter.

Table 19 Properties of W-Zr/MMT 375 and W-Pt/MMT 375 catalysts compared with W/MMT 375 catalyst

Catalyst	BET surface area ^a (m ² /g)	Pore volume ^b (cm ³ /g)	Pore diameter ^b (nm)
W/MMT 375	113.6	0.185	4.7
W-Zr/MMT 375	88.9	0.173	5.3
W-Pt/MMT 375	136.5	0.216	4.5

^a Determined from BET method ^b Determined from BJH desorption method

The adsorption/desorption isotherms related to the pore structure of W-Zr/MMT 375 and W-Pt/MMT 375, which were analyzed by the N₂ adsorption-desorption isotherms are shown in **Figure 19** and **Figure 20**, respectively. For the catalysts of both promoters, they exhibited the type IV isotherm with type H3 hysteresis loop according to IUPAC classification (International Union of Pure and Applied Chemistry) [39], and capillary condensation in the pores at relative pressure (P/P_0) approach 0.40. Type IV isotherms are given by mesoporous adsorbents.

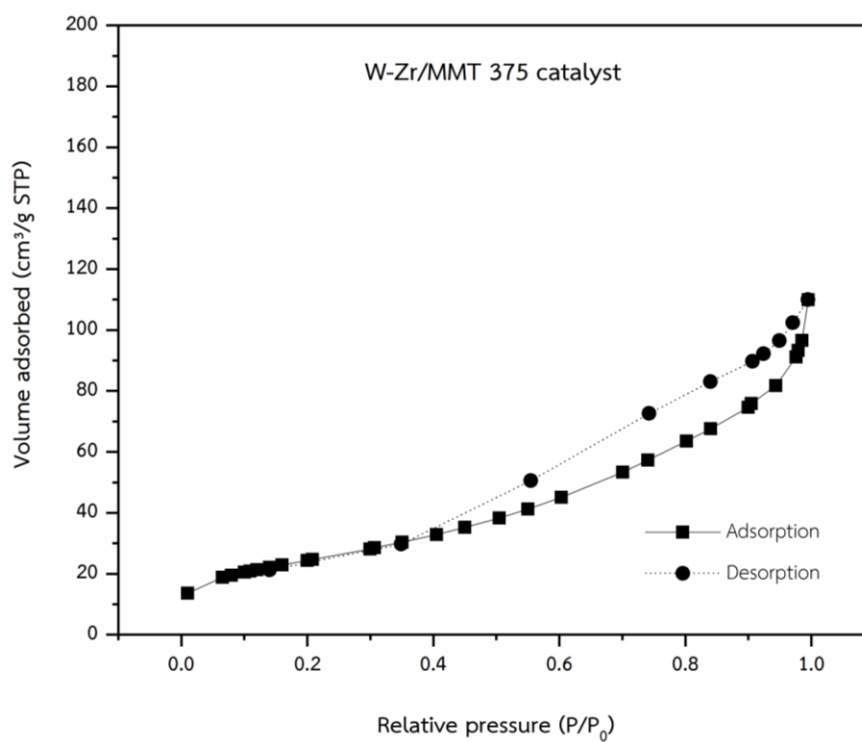


Figure 19 N_2 adsorption-desorption isotherm of W-Zr/MMT 375

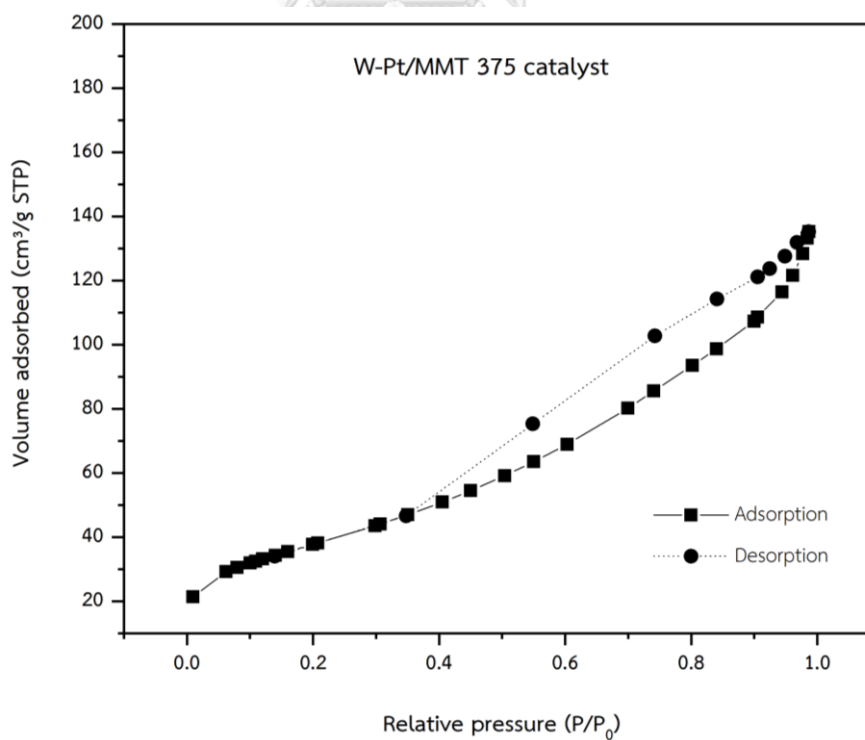


Figure 20 N_2 adsorption-desorption isotherm of W-Pt/MMT 375

4.2.1.4 Scanning electron microscope (SEM) and Energy dispersive X-ray spectroscopy (EDX)

The morphologies of the W-Zr/MMT 375 and W-Pt/MMT 375 catalysts were analyzed by scanning electron microscope (SEM) as shown in **Figure 21**. For the **Figure 21(a)** and **Figure 21(b)**, they were presented morphologies of W-Zr/MMT 375 catalyst at mag. X6,000 and X2,000, respectively. It was found that the particle of Zr (predict) stucked to the catalyst surface in a partially dense bonding manner. The morphologies of W-Pt/MMT 375 catalyst are shown in **Figure 21(c)** and **Figure 21(d)** at mag. X6,000 and X2,000, respectively. It was found that the particle of Pt (predict) replaced the surface area and distributed in the pores.

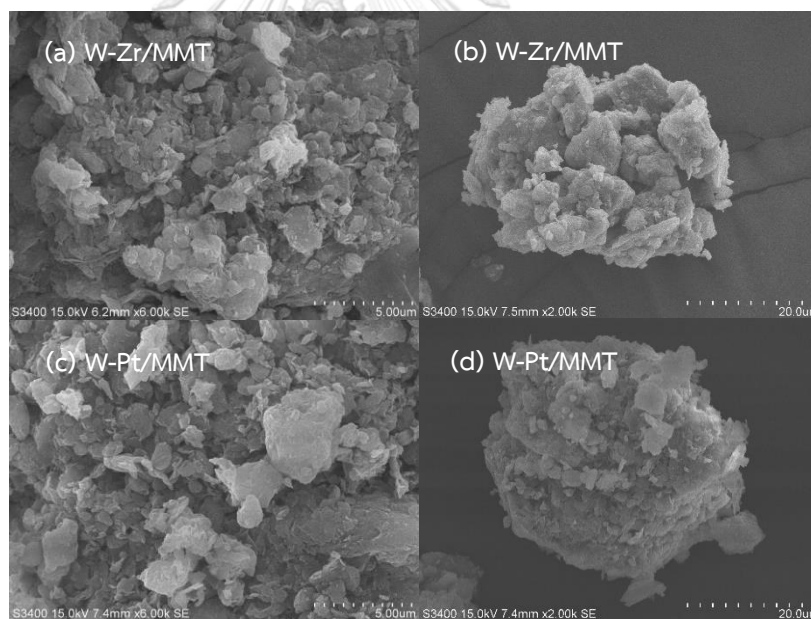


Figure 21 The morphologies of various promoter Zr and Pt for synthesized catalyst tungsten supported on montmorillonite (W-Zr/MMT, W-Pt/MMT) calcined at temperature 375 °C measured by SEM at mag. X6,000 (top and bottom left) and at mag. X2,000 (top and bottom right)

The elemental distribution of all catalysts can be quantitatively analyzed by energy dispersive X-ray spectroscopy (EDX) as shown in **Table 20**. The % weight of elemental distribution of the W-Zr/MMT 375 catalyst consisted of W (45.48), O (23.57) and Zr (23.34), while the W-Pt/MMT 375 catalyst exhibited the highest % weight of W (56.18) and O (29.63). However, it showed the Pt wt% was approximately 0.36.

Table 20 Element distribution of W-Zr/MMT 375 and W-Pt/MMT 375 catalysts

Catalyst	% Weight									
	N	O	Na	Mg	Al	Ca	W	C	Zr	Pt
W-Zr/MMT 375	3.64	23.57	0.18	0.27	3.01	0.51	45.48	-	23.34	-
W-Pt/MMT 375	0.75	29.63	0.37	0.71	11.08	0.19	56.18	0.75	-	0.36

4.2.1.5 Temperature-programmed desorption of ammonia (NH₃-TPD)

The amount of acidity of all catalysts can be determined by integration of desorption area of ammonia according to the Gauss curve fitting method and it is presented in **Table 21**. It was found that W-Pt/MMT 375 catalyst exhibited the highest amount of moderate to strong acid site and total acid site than W-Zr/MMT 375.

Table 21 The amount of acidity of W-Zr/MMT 375 and W-Pt/MMT catalysts by NH₃-TPD

Catalyst	Acidity (μmol NH ₃ /g)		
	Weak	Moderate to strong	Total acid site
W-Zr/MMT	423.0	2431.8	2854.8
W-Pt/MMT	645.5	2775.2	3420.7

4.2.1.6 X-ray photoelectron spectroscopy (XPS)

The X-ray photoelectron result of the W-Zr/MMT 375 catalyst is presented in **Table 22**. The Zr 3d signal around 178 eV was added from original (Table 15 of W/MMT catalysts) and it was assigned to Zr⁴⁺ ions species in ZrO₂ [46]. The result of W-Pt/MMT 375 catalyst is shown in **Table 23**. The Pt 4d and Pt 4f signals was observed at 328.4

and 78.5 eV respectively, which were added from original (Table 15 of W/MMT catalysts) and can be assigned to Pt²⁺ ions [50].

Table 22 XPS signals distribution of W-Zr/MMT 375

Binding energy (eV)									
Na	O	N	Ca	C	Zr	Al	W	W	Mg
1s	1s	1s	2p	1s	3d	2p	4f1	4f2	2s
1082	533.8	401.3	351.7	285	178	76.5	39	27.5	96.4

Table 23 XPS signals distribution of W-Pt/MMT 375

Binding energy (eV)											
Na	O	N	Ag	Ca	Pt	C	Mg	Al	Pt	W	W
1s	1s	1s	3d	2p	4d	1s	2p	2p	4f	4f1	4f2
1083.9	535.1	399.4	368.2	348.6	328.4	286.1	96.0	77.5	78.5	39.6	28.7

The surface compositions of the W-Zr/MMT 375 and W-Pt/MMT catalysts are presented in **Table 24** to **Table 25**. For the W-Zr/MMT 375 catalyst, it showed the mass concentration (%) of the O 1s signal, which was the highest around 50.52 % among all compositions and the Zr 3d signal was around 1.22% as the result of the W-Pt/MMT 375 showing the O 1s signal of 40.23 % that was the highest among others. The Pt 4d and 4f signals were found which the mass concentration around 6.46, 1.78 %, respectively. For both promoters loaded not affecting to state of W due to found range of binding energy of W is nearly same with before promoter loaded.

Table 24 Surface composition of W-Zr/MMT 375

% Mass conc									
Na	O	N	Ca	C	Zr	Al	W	W	Mg
1s	1s	1s	2p	1s	3d	2p	4f1	4f2	2s
1.54	50.52	2.47	1.03	22.09	1.22	5.15	5.23	3.91	6.84

Table 25 Surface composition of W-Pt/MMT 375

% Mass conc											
Na	O	N	Ag	Ca	Pt	C	Mg	Al	Pt	W	W
1s	1s	1s	3d	2p	4d	1s	2p	2p	4f	4f1	4f2
1.49	40.23	1.49	1.66	0.81	6.46	27.85	9.13	4.19	1.78	2.22	2.69

4.2.2 Catalytic activities

The catalytic activities of the W-Zr/MMT 375 and W-Pt/MMT 375 catalysts were measured in esterification of ethanol and lactic acid and compared those with the commercial catalyst Amberlyst-15 and W/MMT 375 catalyst (from previous part). The result showed that the W-Pt/MMT 375 catalyst exhibited higher yield of ethyl lactate (ca.48 %) and the W-Zr/MMT 375 catalyst (ca.44 %) as seen in **Figure 22**. Although W-Pt/MMT 375 had the high yield of ethyl lactate, its activity was still lower than Amberlyst-15 (ca.57.8%). Thus, in this part, it can be summarized that the W-Pt/MMT 375 catalyst is the best synthesized catalyst in this study.

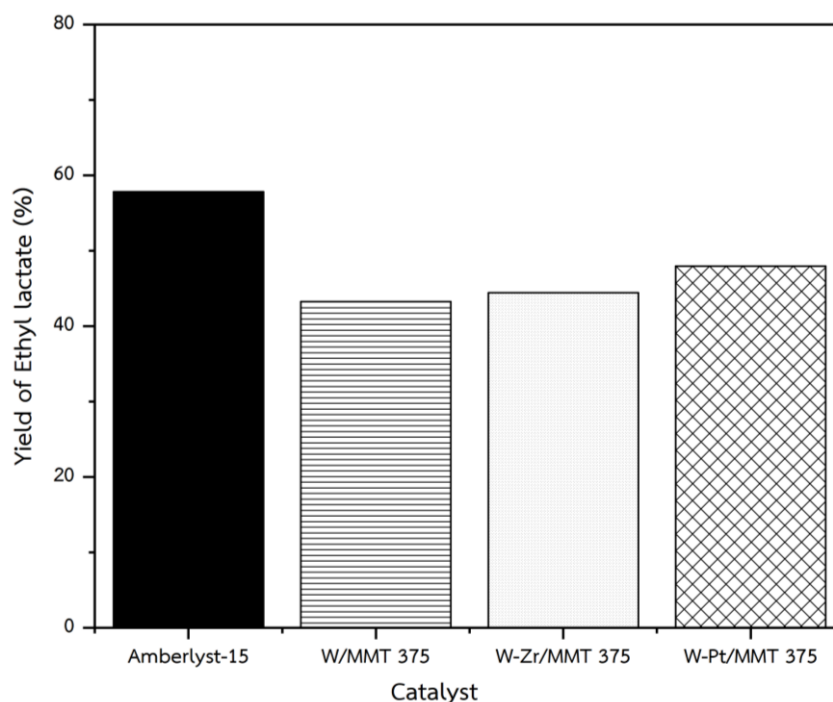


Figure 22 The comparison of yield of ethyl lactate between Amberlyst-15 with W/MMT 375, W-Zr/MMT 375 and W-Pt/MMT 375

4.2.3 Summary

After the reaction test of tungsten supported on montmorillonite clay (W/MMT) catalyst including W-Zr/MMT 375 and W-Pt/MMT 375, the different ethyl lactate yield was observed. It was found from the characterization studies that the W-Pt/MMT 375 catalyst exhibited higher acidity and surface area than the W-Zr/MMT 375 catalyst. As well as, the reaction test results, it revealed higher ethyl lactate yield (48%) obtained from W-Pt/MMT 375 than that of W-Zr/MMT 375. On the other hand, the increase of the yield with Pt promoter was around 11.1% compared with W/MMT 375. However, the W-Zr/MMT375 catalyst was found to give the yield of ethyl lactate around 44.4%, increase only 3% based on W/MMT 375). Consequently, it concluded that the W-Pt/MMT 375 catalyst is the best catalyst for ethyl lactate production based on all synthesized catalysts in this study.

4.3 The study of stability of catalysts

4.3.1 Catalytic stability

The catalytic activity of catalysts such as W/MMT 375 (the best result in part 4.1) and W-Pt/MMT (the best result in part 4.2) was compared with the commercial catalyst Amberlyst-15 from esterification of ethanol and lactic acid. All catalysts were reused for 3 times in the reaction test and the results are presented in **Figure 23**. Considering Amberlyst-15, it exhibited the highest yield of ethyl lactate of 57.8% for the first use and after 3rd reuse the yield of ethyl lactate was dropped to 10.2%. For the W/MMT 375, the ethyl lactate yield of 43.2% was observed at the first use, but after 3 times of reuse, it decreased to 17.9%. In addition, W-Pt/MMT had the yield of ethyl lactate of 48% and it decreased to 14.8% after it was tested for 3 times. Therefore, the reusability of W/MMT 375 and W-Pt/MMT was better than Amberlyst-15 as shown in **Figure 24**. It should be noted that after 3 time-reuse in the reaction test, the ethyl lactate yield was decreased by 82% for Amberlyst-15, whereas they were decreased by 59 and 69% for W/MMT 375 and W-Pt/MMT 375 catalysts, respectively.

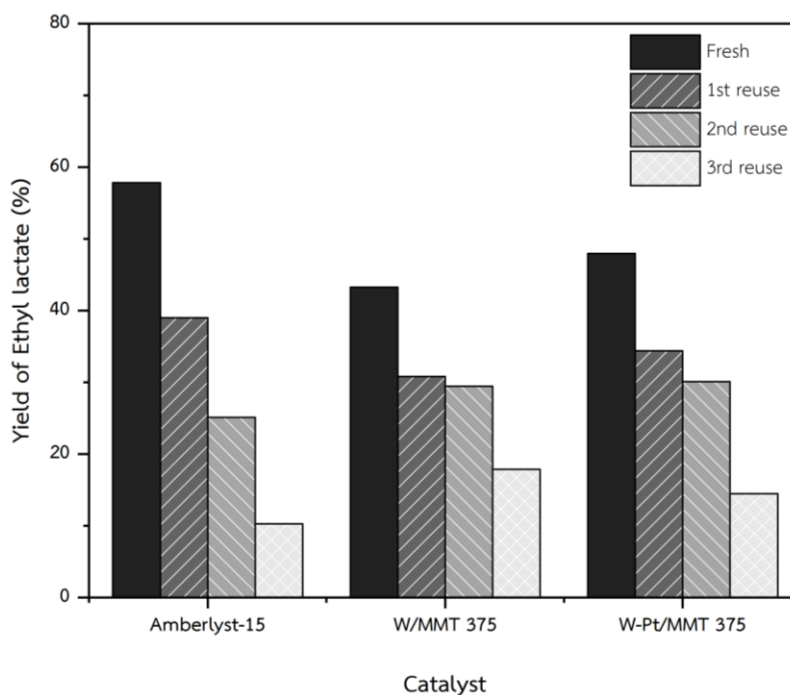


Figure 23 The comparison of yield of ethyl lactate between Amberlyst-15 with W/MMT 375 and W-Pt/MMT 375 from the fresh, 1st reuse, 2nd reuse and 3rd reuse catalyst in esterification

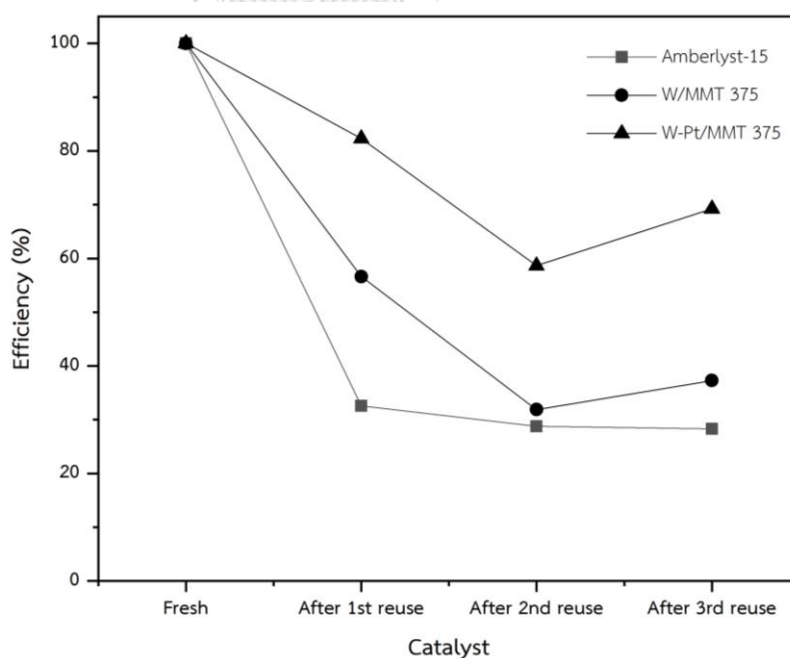
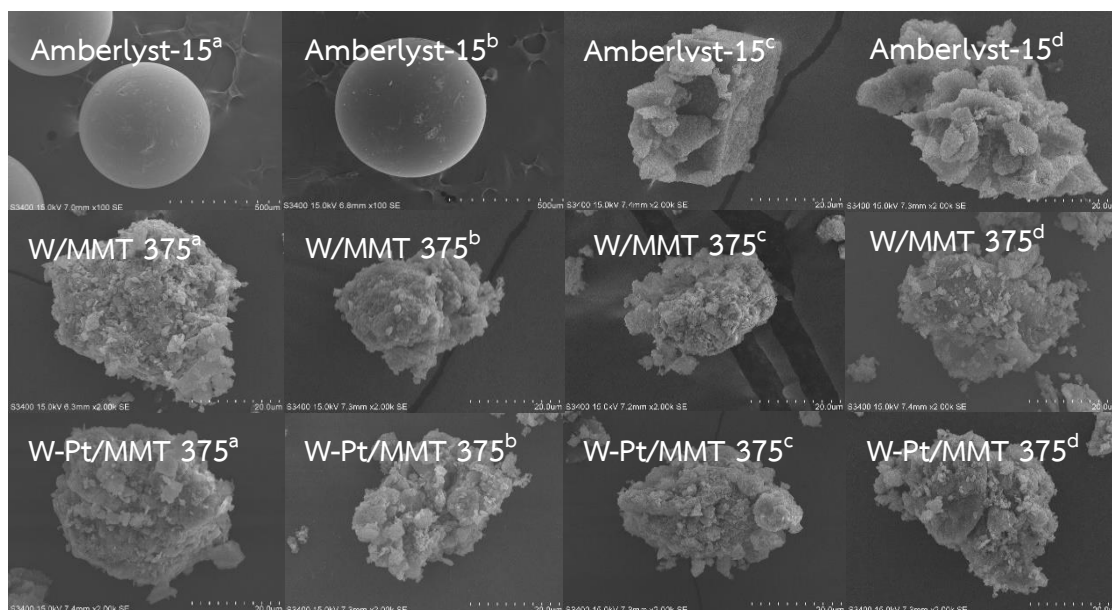


Figure 24 The comparison of an efficiency of catalyst reusability in ethyl lactate production between Amberlyst-15 with W/MMT 375 and W-Pt/MMT 375 from the fresh, 1st reuse, 2nd reuse and 3rd reuse in esterification

4.3.2 Catalyst characterizations

4.3.2.1 Scanning electron microscope (SEM)

The morphologies of all catalysts including W/MMT 375 and W-Pt/MMT 375 compared to the commercial Amberlyst-15 catalyst, which were tested in the reaction for 3 cycles in esterification of ethanol and lactic acid at 80 °C for 4 hours were analyzed by scanning electron microscope (SEM) as shown in **Figure 25**. For Amberlyst-15 catalyst, the results are shown in **Figure 25** revealing the morphologies of Amberlyst-15^a and **Figure 25** Amberlyst-15^b of fresh and first time reuse, respectively. It indicated that at mag. X100 the preliminary particle is spherical having diameter of approximately 0.5 mm. After reaction test in each time, the surface of catalyst was broken, which was occurred from the effect of swelling properties. In addition, the swelling properties occur from the cross-linked of Amberlyst-15 was damage [15]. Amberlyst-15 after the reaction test for 2 times, it was found to change from spherical particle at first time to the irregular shape as shown in **Figure 25** for Amberlyst-15^c and **Figure 25** for Amberlyst-15^d, which are assigned after test of reaction for 2 times and 3 times, respectively. For all synthesized catalysts including W/MMT 375 and W-Pt/MMT 375, the fresh catalysts were powder. After tested in the reaction, the morphologies of all catalysts did not change from the fresh ones. Therefore, the reuse of W/MMT 375 and W-Pt/MMT 375 catalysts by esterification of ethanol and lactic acid did not affect to the morphologies of catalysts.



a represent the fresh catalyst b represent the 1st reuse catalyst
 c represent the 2nd reuse catalyst d represent the 3rd reuse catalyst

Figure 25 The morphologies of all catalysts after tested in the reaction around 3 cycles measured by SEM at mag. X100 (For both of Amberlyst-15^a and Amberlyst-15^b) and at mag. X2,000

4.3.2.2 Temperature-programmed desorption of ammonia (NH₃-TPD)

The temperature-programmed desorption of ammonia of W/MMT 375 and W-Pt/MMT 375 catalysts after tested in the reaction in each reuse is summarized as shown in **Table 26**. All catalysts after tested in the reaction in each reuse had loss their weak and strong acid sites. Thus, the decrease in catalytic activity from the catalysts in each recycle was because the weak and strong acid site were decreased.

Table 26 The amount of acidity of all catalysts for 3 cycles of reuse as W-Zr/MMT 375 and W-Pt/MMT catalysts obtained by NH₃-TPD

Catalyst	Acidity ($\mu\text{mol NH}_3/\text{g}$)		
	Weak	Moderate to strong	Total acid site
W/MMT 375 1 st reuse	186.8	870.4	1057.2
W/MMT 375 2 nd reuse	133.1	564.2	697.3
W/MMT 375 3 rd reuse	98.3	289.1	387.4
W-Pt/MMT 375 1 st reuse	442.8	2091.2	2534.0
W-Pt/MMT 375 2 nd reuse	176.6	1923.7	2100.3
W-Pt/MMT 375 3 rd reuse	121.1	1035.9	1157.0

4.3.3 Summary

Based on the comparison of the stability for catalysts, it was found that the yields of ethyl lactate after 3 cycle-reaction test 3 times of all catalysts were decreased. For Amberlyst-15, the reusability was decreased by 82% after the 3 cycles, whereas the reusability of W/MMT 375 (decreased by 58%) and W-Pt/MMT 375 (decreased by 69.2%) was observed. The morphologies of Amberlyst-15 apparently changed from spherical particle to powder after reuse. On contrary, the morphologies of W/MMT 375 and W-Pt/MMT 375 did not change after reuse. Based on the results from NH₃-TPD, it revealed that the decreased activity for all catalyst was mainly due to the loss in acidity. The acidity of all catalysts was decreased mainly due to leaching.

CHAPTER 5

CONCLUSION AND RECOMMENDATION

In this research, characteristics, catalytic properties and stability of tungsten oxide (13.5 wt%) supported on montmorillonite (W/MMT) catalysts calcined at different temperatures with the presence of Zr and Pr promoters in esterification of ethanol and lactic acid were examined. Consequently, this chapter is summarized all the results in section 5.1 and recommendations about this research in section 5.2.

5.1 Conclusions

5.1.1 For the optimal calcination temperatures selection, the results received from characterization, The surface area of catalyst significantly decreased with increased calcination temperature resulting in low distribution. For catalytic activity, the yield of ethyl lactate is significantly influenced by the high acidity and high surface area of catalyst. For catalyst W/MMT 375, W/MMT 475 and W/MMT 575, ethyl lactate yields are 43.2, 37.3, 33.3% respectively. Therefore, W/MMT 375 was selected to load promoters.

5.1.2 For the suitable promoter selection, the results received from characterization studies showed that the W-Pt/MMT 375 catalyst exhibited the highest acidity and surface area than W-Zr/MMT 375 as well as the reaction test result, which revealed that W-Pt/MMT 375 provided the highest yield of ethyl lactate around 48% (increase by 11.1% compared with W/MMT 375). However, the W-Zr/MMT375 catalyst exhibited the yield of ethyl lactate around 44.4% (increase by 3% compared with W/MMT 375). Consequently, the W-Pt/MMT 375 was selected for the suitable promoter selection.

5.1.3 The catalytic stability was performed around 3 cycles in esterification of ethanol and lactic acid at 80 °C. It was found that W/MMT 375 catalyst had the highest efficiency of decreasing of the yield of ethyl lactate around 58.6%, in descending order

was the W-Pt/MMT 375 catalyst was decreased the efficiency of the yield of ethyl lactate around 69.2%. For Amberlyst-15, it showed the lowest efficiency of decreasing of the yield of ethyl lactate around 82.3% which was corresponding to the result of SEM. The morphology of Amberlyst-15 was damaged and change from original one. Nevertheless, the morphologies of W/MMT 375 and W-Pt/MMT 375 catalysts did not change. Finally, the amount of acidity of catalysts were decreased mainly due to leaching when performed around 3 cycles in esterification of ethanol and lactic acid.

5.2 Recommendations

5.2.1 The pyridine-adsorbed IR spectra should be used to examine types of acidity in catalysts including Lewis acid site and Brønsted acid site.

5.2.2 To examine another promoter for improvement activity and consider comparison about cost.

5.2.3 To apply the catalyst for esterification of ethanol and another carboxylic acid such as propionic acid.

REFERENCES



จุฬาลงกรณ์มหาวิทยาลัย
CHULALONGKORN UNIVERSITY

1. Sorapipatana, C. and S. Yoosin, *Life cycle cost of ethanol production from cassava in Thailand*. Renewable and Sustainable Energy Reviews, 2011. **15**(2): p. 1343-1349.
2. ENERGY, M.O., *Biofuel Strategy for Transportation Sector*. Global Status Report, 2015: p. 11-30.
3. Pereira, C.S.M. and A.E. Rodrigues, *Chapter 6 Ethyl Lactate Main Properties, Production Processes, and Applications*. Green Chemistry and Sustainable Technology, 2014: p. 107-125.
4. Nagendrappa, G.J.R., *Organic synthesis using clay catalysts: Clays for "green chemistry"*. 2002. **7**(1): p. 64-67.
5. Santato, C., M. Ulmann, and J.J.T.J.o.P.C.B. Augustynski, *Photoelectrochemical properties of nanostructured tungsten trioxide films*. 2001. **105**(5): p. 936-940.
6. Ramu, S., et al., *Esterification of palmitic acid with methanol over tungsten oxide supported on zirconia solid acid catalysts: effect of method of preparation of the catalyst on its structural stability and reactivity*. Applied Catalysis A: General, 2004. **276**(1-2): p. 163-168.
7. Zhang, C., et al., *Zeolitic acidity as a promoter for the catalytic oxidation of toluene over MnO /HZSM-5 catalysts*. Catalysis Today, 2019. **327**: p. 374-381.
8. Nguyen, V.C., et al., *Esterification of aqueous lactic acid solutions with ethanol using carbon solid acid catalysts: Amberlyst 15, sulfonated pyrolyzed wood and graphene oxide*. Applied Catalysis A: General, 2018. **552**: p. 184-191.
9. Kua, Y.L., et al., *Ethyl lactate as a potential green solvent to extract hydrophilic (polar) and lipophilic (non-polar) phytonutrients simultaneously from fruit and vegetable by-products*. Sustainable Chemistry and Pharmacy, 2016. **4**: p. 21-31.
10. Pereira, C.S.M., V.M.T.M. Silva, and A.E. Rodrigues, *Ethyl lactate as a solvent: Properties, applications and production processes – a review*. Green Chemistry, 2011. **13**(10).
11. Li, S., et al., *Catalytic conversion of cellulose-based biomass and glycerol to lactic acid*. Journal of Energy Chemistry, 2019. **32**: p. 138-151.

12. Komesu, A., et al., *Lactic acid production to purification: a review*. 2017. **12**(2): p. 4364-4383.
13. Datta, R. and M. Henry, *Lactic acid: recent advances in products, processes and technologies — a review*. *Journal of Chemical Technology & Biotechnology*, 2006. **81**(7): p. 1119-1129.
14. Pal, R., *Amberlyst-15 in organic synthesis*. *ARKIVOC*, 2015: p. 570-609.
15. Wang, Z., et al., *A Cross-Linked and Swelling Polymer as an Effective Solid Acid Catalyst*. *Industrial & Engineering Chemistry Research*, 2015. **54**(29): p. 7219-7225.
16. Massaro, M., et al., *Covalently modified nanoclays: synthesis, properties and applications*, in *Clay Nanoparticles*. 2020. p. 305-333.
17. Zhou, C., D. Tong, and W. Yu, *Smectite Nanomaterials: Preparation, Properties, and Functional Applications*, in *Nanomaterials from Clay Minerals*. 2019. p. 335-364.
18. Christian, J.B. and M.S. Whittingham, *Structural study of ammonium metatungstate*. *Journal of Solid State Chemistry*, 2008. **181**(8): p. 1782-1791.
19. Guan, W., et al., *Preliminary study on preparation of ammonium metatungstate from ammonium tungstate solutions using bipolar membrane electrodialysis*. *Hydrometallurgy*, 2017. **169**: p. 239-244.
20. Guguloth, V.C. and S. Battu, *Synthesis of Some Aromatic and Aliphatic Esters Using WO₃/ZrO₂ Solid Acid Catalyst under Solvent Free Conditions*. *Asian Journal of Chemistry*, 2020. **32**(9): p. 2153-2157.
21. F.T. Zangeneh, S.S., *Effect of Addition of Different Promoters on the Performance of Pt-Sn-K/Al₂O₃ Catalyst in the Propane Dehydrogenation* *Iranian Journal of Chemical Engineering*, 2011. **8**: p. 48-54.
22. Yu, W., et al., *Acid-activated and WO₃-loaded montmorillonite catalysts and their catalytic behaviors in glycerol dehydration*. *Chinese Journal of Catalysis*, 2017. **38**(6): p. 1087-1100.

23. Ma, J., et al., *Intensifying esterification reaction between lactic acid and ethanol by pervaporation dehydration using chitosan–TEOS hybrid membranes*. Chemical Engineering Journal, 2009. **155**(3): p. 800-809.
24. Pereira, C.S.M., et al., *Thermodynamic Equilibrium and Reaction Kinetics for the Esterification of Lactic Acid with Ethanol Catalyzed by Acid Ion-Exchange Resin*. Ind. Eng. Chem. Res. 2, 2008. **47**: p. 1453-1463.
25. Lopez, D., et al., *Esterification and transesterification on tungstated zirconia: Effect of calcination temperature*. Journal of Catalysis, 2007. **247**(1): p. 43-50.
26. Yu, J., et al., *Effect of calcination temperatures on microstructures and photocatalytic activity of tungsten trioxide hollow microspheres*. J Hazard Mater, 2008. **160**(2-3): p. 621-8.
27. Gao, H., et al., *Fe–Ni–Al pillared montmorillonite as a heterogeneous catalyst for the Catalytic Wet Peroxide Oxidation degradation of Orange Acid II: Preparation condition and properties study*. Microporous and Mesoporous Materials, 2014. **196**: p. 208-215.
28. Jiang, B., et al., *Highly dispersed Ni/montmorillonite catalyst for glycerol steam reforming: Effect of Ni loading and calcination temperature*. Applied Thermal Engineering, 2016. **109**: p. 99-108.
29. Schott, F.J.P., et al., *Reduction of NO_x by H₂ on Pt/WO₃/ZrO₂ catalysts in oxygen-rich exhaust*. Applied Catalysis B: Environmental, 2009. **87**(1-2): p. 18-29.
30. Hernandez-Pichardo, M.L., et al., *High-throughput study of the iron promotional effect over Pt/WO_x–ZrO₂ catalysts on the skeletal isomerization of n-hexane*. Applied Catalysis A: General, 2012. **431-432**: p. 69-78.
31. liewchalermwong, J., *Catalytic dehydration of ethanol with different loading of WO₃ supported on activated carbon and clay catalysts [Thesis]*. 2019: p. 17-18.
32. Djowe, A.T., et al., *Surface Modification of Smectite Clay Induced by Non-thermal Gliding Arc Plasma at Atmospheric Pressure*. Plasma Chemistry and Plasma Processing, 2013. **33**(4): p. 707-723.

33. Kalhori, H., et al., *Flower-like nanostructures of WO₃: Fabrication and characterization of their in-liquid gasochromic effect*. Sensors and Actuators B: Chemical, 2016. **225**: p. 535-543.
34. Szilágyi, I.M., et al., *Preparation of hexagonal WO₃ from hexagonal ammonium tungsten bronze for sensing NH₃*. Materials Research Bulletin, 2009. **44**(3): p. 505-508.
35. Danková, Z., A. Mockovčíaková, and S. Dolinská, *Influence of ultrasound irradiation on cadmium cations adsorption by montmorillonite*. Desalination and Water Treatment, 2013. **52**(28-30): p. 5462-5469.
36. Ahmed, A., et al., *XRD and ATR/FTIR investigations of various montmorillonite clays modified by monocationic and dicationic imidazolium ionic liquids*. Journal of Molecular Structure, 2018. **1173**: p. 653-664.
37. MOHANTA, V.B.K.a.D., *Formation of nanoscale tungsten oxide structures and colouration characteristics*. Indian Academy of Sciences, 2011. **34**: p. 435-422.
38. Tuchowska, M., et al., *Sorption of Molybdates and Tungstates on Functionalized Montmorillonites: Structural and Textural Features*. Materials (Basel), 2019. **12**(14).
39. Thommes, M., et al., *Physisorption of gases, with special reference to the evaluation of surface area and pore size distribution (IUPAC Technical Report)*. Pure and Applied Chemistry, 2015. **87**(9-10): p. 1051-1069.
40. Krutpijit, C. and B. Jongsomjit, *Catalytic Ethanol Dehydration over Different Acid-activated Montmorillonite Clays*. J Oleo Sci, 2016. **65**(4): p. 347-55.
41. Liu, D., et al., *Quantitative characterization of the solid acidity of montmorillonite using combined FTIR and TPD based on the NH₃ adsorption system*. Applied Clay Science, 2013. **80-81**: p. 407-412.
42. Gonçalves, V.L.C., et al., *Acetylation of glycerol catalyzed by different solid acids*. Catalysis Today, 2008. **133-135**: p. 673-677.
43. S. Bensalem, B.H., Sylvie del Confetto, M. Iguer-Ouada, Alain and H.B. Chamayou, Rachel Calvet, *Characterization of chitosan/montmorillonite bionanocomposites by inverse gas chromatography*. 2018.

44. Detoni, C., A.R.P. da Silva, and M.M.V.M. Souza, *Effect of Pt/HZSM-5 dealumination by high temperature reduction on glycerol oxidation*. Journal of Porous Materials, 2020. **27**(3): p. 707-717.
45. Al-Kandari, H., et al., *Surface electronic structure–catalytic activity relationship of partially reduced WO₃ bulk or deposited on TiO₂*. Journal of Electron Spectroscopy and Related Phenomena, 2006. **151**(2): p. 128-134.
46. Jahangiri, H., et al., *Zirconia catalysed acetic acid ketonisation for pre-treatment of biomass fast pyrolysis vapours*. Catalysis Science & Technology, 2018. **8**(4): p. 1134-1141.
47. D. M. Ferrer, J.A.M.B., M.L.M. U. P. García, and R.S. Rodrigo, *Electrochemical evaluation of Pt/GMC and Pt/rGO for the electro-oxidation of methanol*. 2016.
48. Balouch, A., et al., *Synthesis of amorphous platinum nanofibers directly on an ITO substrate and its heterogeneous catalytic hydrogenation characterization*. ACS Appl Mater Interfaces, 2015. **7**(14): p. 7776-85.
49. Karim, A.H., et al., *WO₃ monolayer loaded on ZrO₂: Property–activity relationship in n-butane isomerization evidenced by hydrogen adsorption and IR studies*. Applied Catalysis A: General, 2012. **433-434**: p. 49-57.
50. Jeong, Y.E., et al., *Catalytic Activity and Thermal Stability of Arc Plasma Deposited Pt Nano-Particles on CeO₂-Al₂O₃*. J Nanosci Nanotechnol, 2015. **15**(11): p. 8494-501.



APPENDIX A

CALCULATION OF ACID SITE CATALYST

Calculation of acidity

The acidity was determined by NH_3 -TPD, it can be calculated from NH_3 -TPD profile as follow.

$$\text{Acidity of catalysts} = \text{mol of } \text{NH}_3 \text{ desorption per } g_{\text{Cat}} \quad (\text{A.1})$$

Upon, g_{Cat} was weight of dry catalyst

To calculate mole of NH_3 desorption from the calibration curve of NH_3 as follow:

$$\text{mol of } \text{NH}_3 \text{ desorption per } g_{\text{Cat}} = 2.628 \times 10^{-5} \times A \quad (\text{A.2})$$

Where, A was area under peak per weight of dry catalyst of the NH_3 -TPD profile. Then combine equation (A.1) and (A.2). So, the equation (A.1) can be take place as equation (A.3)

$$\text{Acidity of catalysts} = 2.628 \times 10^{-5} \times A \quad (\text{A.3})$$

Example of curve fitting by Fityk program :

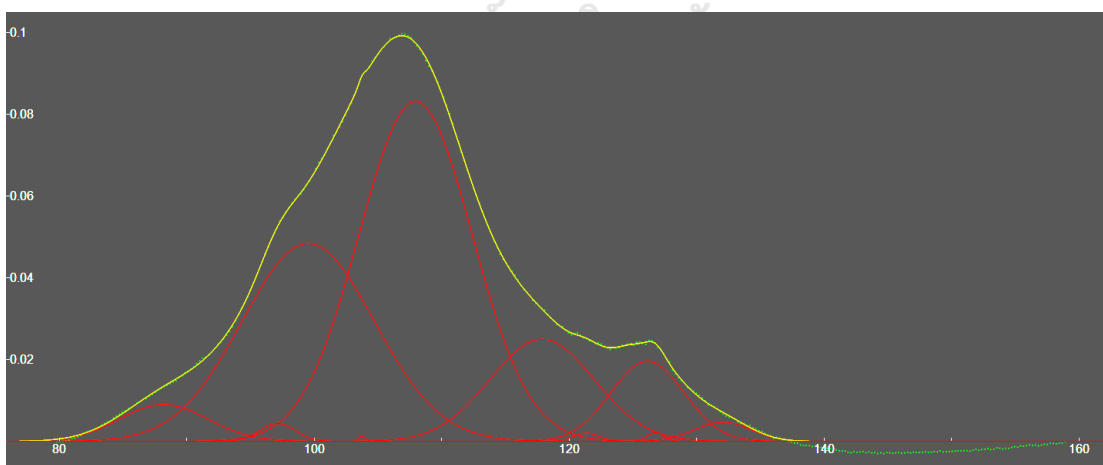


Figure A.1 TCD-time curve fitting of W/MMT 375 catalyst by Gaussian curve in Fityk program

APPENDIX B

CALIBRATION CURVE OF REACTANT AND PRODUCT

Calibration curves were used calculation mole of ethanol, lactic acid and ethyl lactate were presented in Figure B.1-B.3. The concentration of there were measured by Shimadzu gas chromatography with flame ionization detector (GC-FID) using capillary column (DB-5) at 150 °C. In addition, the reaction retention time of each composition is indicated in **Table B.1**.

Table B.1 The retention times analysis of each component in GC-FID

Reactant / Product	Retention time (min)
Ethanol	2.6
Lactic acid	7.0
Ethyl lactate	7.4

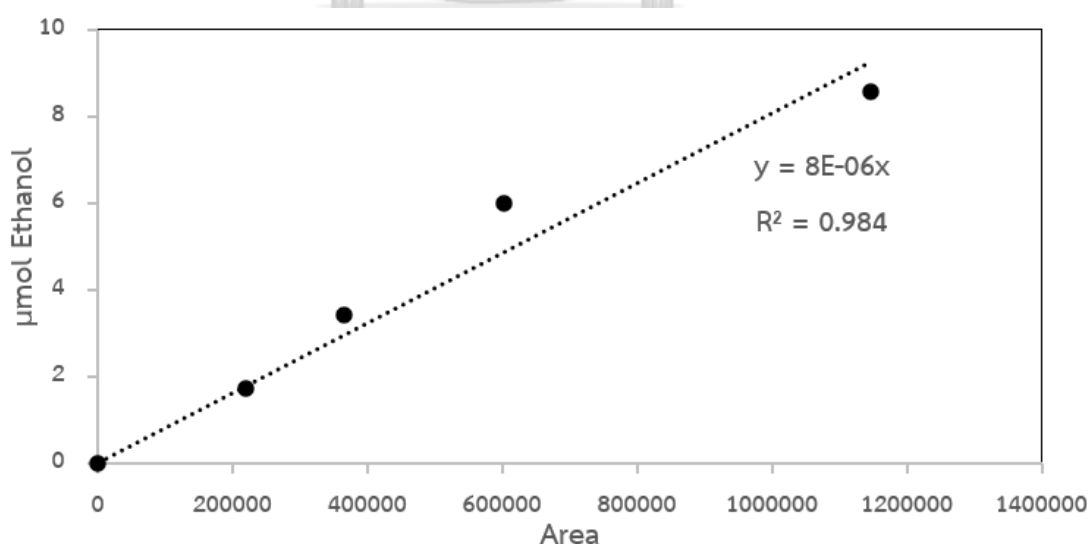


Figure B.1 The calibration curve of Ethanol

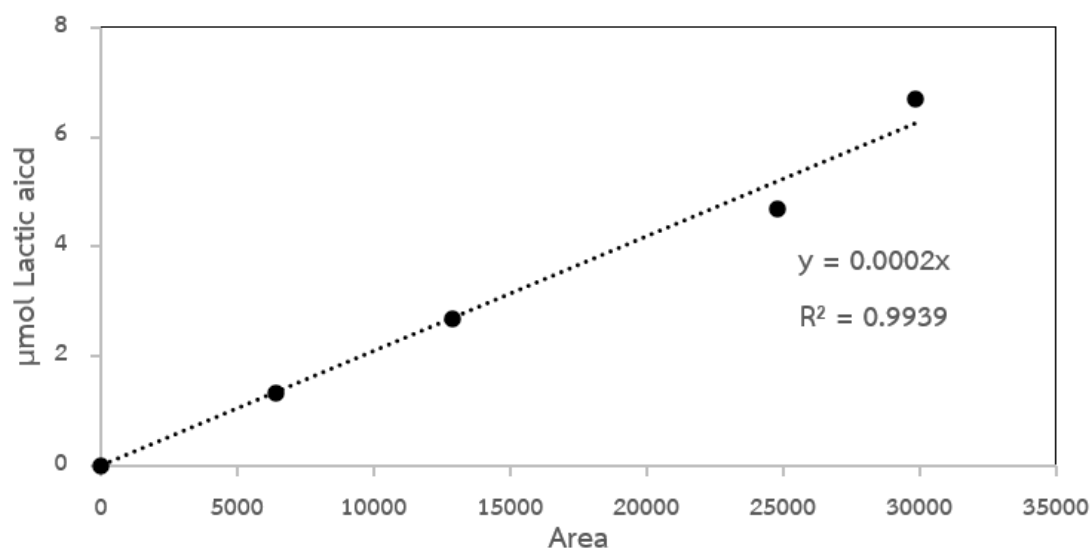


Figure B.2 The calibration curve of Lactic acid

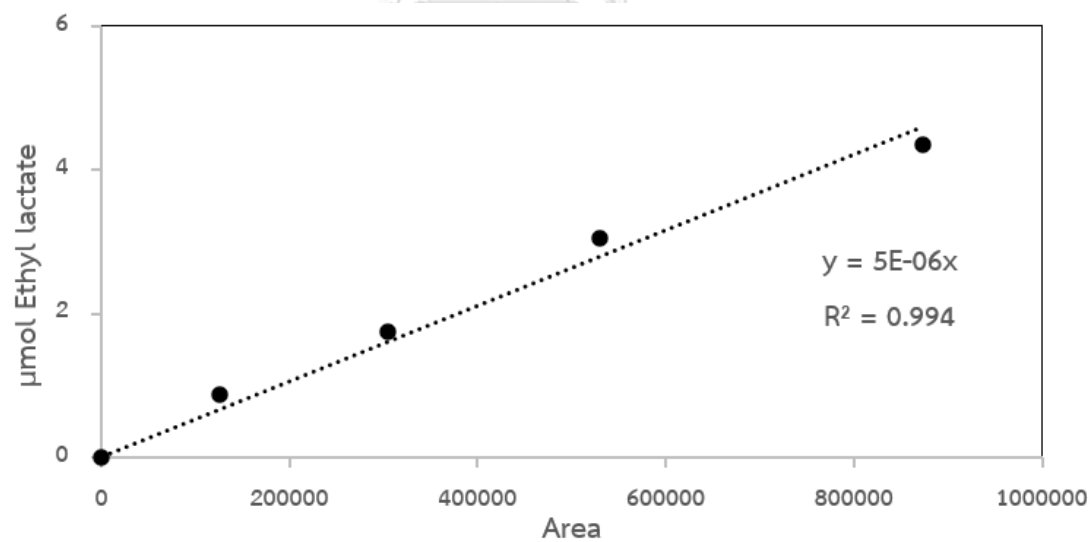


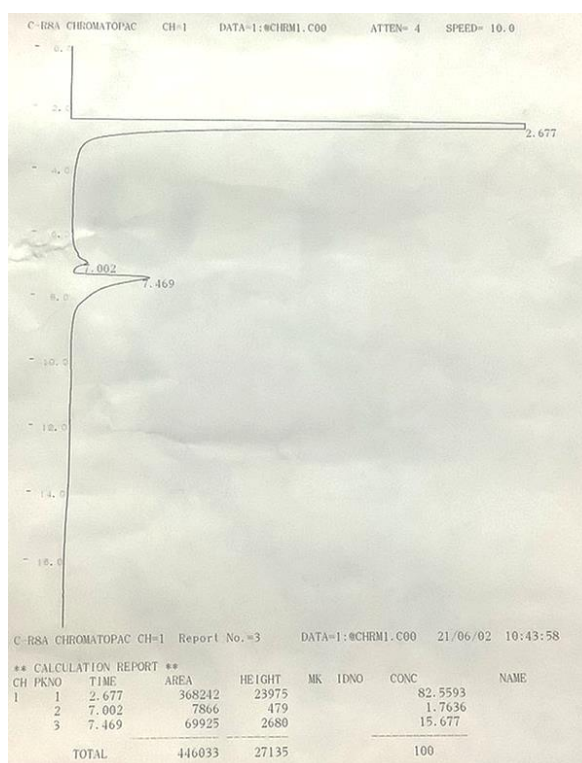
Figure B.3 The calibration curve of Ethyl lactate

From calibration curve ;

$$\mu\text{mole of Ethanol} = (8 \times 10^{-6}) \times \text{Area}$$

$$\mu\text{mole of Lactic acid} = (2 \times 10^{-4}) \times \text{Area}$$

$$\mu\text{mole of Ethyl lactate} = (5 \times 10^{-6}) \times \text{Area}$$



CHULALONGKORN UNIVERSITY
Figure B.4 The GC result

Example ;

From Figure B.4, the area of reactant and product can be detected by gas chromatography (GC-FID). The peak at 2.677 min represents area of ethanol, while peak at 7.002 and 7.496 min shown area of lactic acid and ethyl lactate, respectively.

$$\text{Thus, mole of ethyl lactate} = (5 \times 10^{-6}) \times 69925$$

$$= 0.35 \mu\text{mole}$$

APPENDIX C

CALCULATION OF REACTANT AND CATALYST

Molar ration of ethanol and lactic acid at 3: 1

- Density of ethanol = 0.789 g/mL
- Density of lactic acid = 1.209 g/mL
- Molecular weight of ethanol = 46.07 g/mol
- Molecular weight of lactic acid = 90.08 g/mol

Calculations ;

$$\frac{\text{mol of ethanol}}{\text{mol of lactic acid}} = \frac{3}{1}$$

$$1 \left(\frac{\rho_E V_E}{MW_E} \right) = 3 \left(\frac{\rho_L V_L}{MW_L} \right)$$

$$1 \left(\frac{0.789 \times V_E}{46.07} \right) = 3 \left(\frac{1.209 \times V_L}{90.08} \right)$$

$$0.0171V_E = 0.0403V_L$$

$$0.424V_E = V_L$$

For experiment ;

$$V_E = 35 \text{ mL}$$

$$V_L = 0.424 \times 35 \approx 15 \text{ mL}$$

The catalyst loading is 2%wt of lactic acid

$$\text{Mass of lactic acid} = 15 \text{ mL} \times 1.209 \frac{\text{g}}{\text{mL}} = 18.14 \text{ g}$$

$$\text{Amount of catalyst} = 18.14 \times 0.02 = 0.36 \text{ g}$$

APPENDIX D
THE DATA INFORMATION OF CHARACTERIZATION EQUIPMENT

Table E.1 The characterization data equipment of this research

Technique	Characterization	Contact
XRD	The structure, crystallinity, and physical properties of sample	Center of Excellence on Catalysis and Catalytic Reaction Engineering
FTIR	The functional group of catalysts	SCG-CHULA ENGINEERING Research Center
BET	The BET surface area, pore volume, pore diameter, and adsorption/desorption isotherm	Center of Excellence on Catalysis and Catalytic Reaction Engineering
SEM-EDX	SEM ; Morphology of catalysts EDX ; Element of catalysts	Center of Excellence on Catalysis and Catalytic Reaction Engineering
NH ₃ -TPD	The acid strength of sample (weak, medium, and strong acid sites)	SCG-CHULA ENGINEERING Research Center
XPS	The surface element of catalysts	Center of Excellence on Catalysis and Catalytic Reaction Engineering
XRF	Metal composition in sample	Scientific and Technological Research Equipment Center

VITA

NAME Suthicha Mukjinda

DATE OF BIRTH 3 April 1992

PLACE OF BIRTH Kanchanaburi

INSTITUTIONS ATTENDED Bachelor's degree from Faculty of Engineering in Chemical Engineering, Srinakharinwirot University in 2015

HOME ADDRESS 177 Pak Phraek Road, Ban Nuea Sub-district, Muang District, Kanchanaburi, 71000

